COO/2971-1

NATURAL CONVECTION CHARACTERISTICS OF FLAT PLATE COLLECTORS

Progress Report

By
K. R. Randall
M. M. El-Wakil
J. W. Mitchell

Date Published—September 1977

Work Performed Under Contract No. EY-76-S-02-2971

University of Wisconsin
Engineering Experiment Station
Madison, Wisconsin

ENERGY RESEARCH AND DEVELOPMENT ADMINISTRATION
Division of Solar Energy

DISCLAIMER

NOTICE

This report has been reproduced directly from the best available copy.

Available from the National Technical Information Service, U. S. Department of Commerce, Springfield, Virginia 22161

Price: Paper Copy ~~$4.50~~ 5.25 (domestic)
~~$7.00~~ (foreign) 10.50
Microfiche $3.00 (domestic)
$4.50 (foreign)

COO/2971-1
Distribution Category UC-59c

ENGINEERING EXPERIMENT STATION

NATURAL CONVECTION CHARACTERISTICS OF FLAT PLATE COLLECTORS

Progress Report

by
K.R. Randall, M.M. El-Wakil, and J.W. Mitchell

April 1977

Contract E(11-1)-2971

Energy Research & Development Administration

University of Wisconsin
Engineering Experiment Station
Madison, Wisconsin

NATURAL CONVECTION CHARACTERISTICS OF FLAT PLATE COLLECTORS

by

K. R. Randall, M. M. El-Wakil, and J. W. Mitchell

Natural convection heat transfer between parallel plates has been experimentally studied for conditions similar to those existing in flat plate solar collectors. Interferometric techniques have been used to provide detailed information on the local variation of the heat transfer coefficient along the plate surface. Local values have been integrated along the plate length to determine the average heat transfer coefficient. The results are useful in determining the top loss coefficient for flat plate collectors.

Parallel plates tilted between 45° and vertical have been investigated. The aspect ratio (ratio of plate length to plate spacing) and Grashof number are comparable to those for current collector designs.

For the tilt angles and aspect ratios studied, the local heat transfer coefficient is greater than the average by a factor of 2 to 3 at the lower end of the heated plate, and is about one-half the average at the upper end of the heated plate. For low and high Grashof number, the heat transfer coefficient is constant over the center section of the plate, while at intermediate Grashof numbers, it decreases continuously from the lower to the upper end. The limits on Grashof number are a strong function of the enclosure aspect ratio.

The results for angles of tilt between 45 and 70° are consistent with those of previous investigations. The data confirm that the

technique of K.G.T. Hollands, in which only the heat transfer from the center portion of the plate is measured, is a valid method for determining the average coefficient. The center value accurately reflects the average value.

Measured heat transfer coefficients for tilt angles in the range of 70 to 90° help resolve the deficiencies that currently exist in the data. The influence of aspect ratio on the average heat transfer rate is found to be considerably less than previously postulated, with essentially no effect of large aspect ratios.

A correlation is developed for the average heat transfer coefficient in terms of tilt angle, and additional correlations are formulated for the local variations of the heat-transfer coefficient.

CONTENTS

LIST OF FIGURES

NOMENCLATURE

g	acceleration of gravity
h	local heat-transfer coefficient
$\bar{h}$	average heat-transfer coefficient
H	height of air layer
k	thermal conductivity
L	plate spacing
T	temperature
W	width of air layer
X	distance from starting or departure corner
y	distance from the wall
α	thermal diffusivity
β	coefficient of volumetric expansion
ν	kinematic viscosity
ϕ	enclosure tilt angle

Subscripts

c	conduction	m	mean
C	cold	p	penetration
cr	critical	s	starting
d	departure	w	wall (hot or cold)
H	hot	x	based on X
L	based on L		

Non-dimensional Parameters (all properties evaluated at T_{mean})

$Gr_L = g\beta(T_H-T_C)L^3/\nu^2$ -- Grashof number based on L

$Gr_x = g\beta(T_H-T_C)X^3/\nu^2$ -- Grashof number based on X

$\overline{Nu}_L = hL/K$ -- average Nusselt number based on L

$\overline{Nu}_L = hL/K$ -- local Nusselt number based on L

$Nu_x = hX/K$ -- local Nusselt number based on X

$Pr = \nu/\alpha$ -- Prandtl number

$Ra_L = g\beta(T_H-T_C)L^3/\nu\alpha$ -- Rayleigh number based on L

$\overline{y} = y/L$ -- distance from the wall

$\Theta = \frac{T-T_C}{T_H-T_C}$ -- temperature

SUMMARY

This report describes the results of an experimental investigation into the convective heat losses in large aspect ratio flat-plate solar collectors.

An experimental study has been undertaken on a specially designed test cell using a 3 inch Mach-Zehnder interferometer. Air at atmospheric pressure was used as the heat-transfer fluid. The experimental results include inteferograms which show the thermal boundary layer formations and the temperature profiles. Local temperature profiles have been analyzed through the use of an optical comparator to determine local Nusselt number profiles, which have, in turn, been integrated to give average heat-transfer results.

Angles of inclination from the horizontal of 45, 60, 75 and 90 degrees have been investigated. Aspect ratios from 9 to 36 were examined over a Rayleigh number range of 4000 to 310000.

Finally, heat-transfer correlations have been developed for the prediction of local Nusselt numbers in the starting and departure corners and for the average heat-transfer results as a function of collector tilt angle.

1. INTRODUCTION

1.1 The Problem

The free-convective heat transfer across inclined layers has always been of considerable interest. Engineers have been concerned about the determination of heat losses in enclosed spaces such as the airspaces in buildings or in the prediction of nuclear reactor core temperatures. Of particular interest to specific problems of today is the minimization of free-convective heat losses in flat-plate solar collectors.

The analysis of free convection in enclosures has a long history but it has only been recently that great strides have been made in understanding the mechanism by which the heat transfer occurs. Except for the limiting case of vertical and horizontal layers which have been extensively studied, very little information exists on the average heat-transfer phenomena for other angles. Virtually no information exists on the variations of the local heat transfer phenomena in vertical and inclined enclosures.

More recently the results of Hollands et al., (25, 26, 36) on the convective losses in flat-plate collectors have received considerable attention as a correlation representative of current collector performance for inclinations less than about 70 degrees. The Waterloo experimental apparatus has built into the measurement of the heat flow the assumption that the heat transfer near the ends of the enclosure does not contribute significantly to the overall heat transfer. The present investigation, through evaluation of the local variations in the heat transfer coefficients, is able to test the above assumption.

1.2 Literature Survey

1.2.1 Thermal Instability

The initiation of convection in an inclined enclosure occurs when the buoyant forces exceed the viscous forces. The heat transfer below this point is only by the mechanism of conduction while beyond this point (called the critical Rayleigh number, Ra_{cr}) it is augmented by a "top heavy" situation. The buoyancy component of the flow up the slope causes a single cell circulation which has superimposed upon it a rolling motion due to the temperature induced top heavy phenomena.

There is universal agreement, both theoretically and experimentally, that Ra_{cr} for infinite horizontal layers is 1709 [8,9,11,13,14,22, 23,24,25,30,43]. Catton [10] has undertaken a theoretical investigation using the method of B. G. Galerkin [29] to determine the effect of finite cavity size on the initiation of convection. His results show that the effect of confining walls is to suppress the departure from conduction due to the effect of wall shear on fluid motion and that the amount of suppression is a function of both cavity width and length aspect ratios. The results are carried out to only length and width aspect ratios of six at which the critical Rayleigh number is 1992.

Contrary to the results of Catton, Norden and Usmanov [31], in an interferometric study of the critical point in horizontal layers of ethyl alcohol, water, and ehtylene glycol, found that the departure from the conduction regime actually occured at Rayleigh number less than 1700 and that the thinner the layer the lower the value of Ra_{cr}. This disagreement with Catton is attributed by the authors to the effect of the lateral boundaries of the layer.

The most comprehensive experimental determination of the critical Rayleigh number for all angles of tilt was accomplished by Hollands and Konicek [24]. Ra_{cr} was found by measuring the heat flux in close proximity to the conduction regime and extrapolating the results to the conduction limit. The results were found to agree with those of Unny [41] with a maximum deviation of 10%. The resulting data was found to fit the equation

$$Ra_{cr} \cos(\phi) = 1709 \qquad \phi \leq 60$$

For $\phi > 60$, wide variance has been found between experiment and theory, which is due to the inability to detect very weak flows, and no correlation exists which accurately predicts Ra_{cr} for this range of tilt angles.

DeGraaf and Van Der Held [13] were one of the first investigators to visually observe the flow patterns by injecting smoke into the test cavity. They observed the regular cellular convection for Rayleigh number greater than 2000 in the horizontal layer (Bénard cells). A transition into turbulence was noted for Rayleigh number greater than 40000. On turning the air layer from the horizontal to 10 degrees they noted the cellular convection changing to rolls whose axes are perpendicular to the tilt axis (called x-rolls). The x-rolls were noted up to 20 degrees inclination but disappeared thereafter.

The stability equations derived by Unny [41] show that x-rolls are as likely to occur as y-rolls (rolls whose axes are parallel to the tilt axis); but, the rolls are aligned in a preferred direction upon tilting the enclosure. This direction is a function of the

Prandtl number. For small Prandtl number, y-rolls occur, and for large Prandtl number, x-rolls occur. Air is considered by the author to be a large Prandtl number fluid!

Hart [22,23] and Unny [41] have tackled the problem of determining the tilt angle at which there is a crossover from the top-heavy instability associated with x-rolls to the dynamic instability associated with y-rolls. The dynamic instability is found in vertical and near-vertical cavities in which occur buoyancy driven boundary layer flows. Hart found this angle to be 72 degrees while Unny found it to be 78 degrees. This suggests that a fluid in inclined layers of tilt angles less than about 75 degrees has instabilities similar to the horizontal layer and for angles greater than 75 degrees the instabilities are similar to those of the vertical layer.

1.2.2 Inclined Flat Plate Enclosures

A summary of experimental studies on free convection heat transfer in flat plate enclosures bounded by differentially heated isothermal surfaces is presented by Tabor [40] for the pre-1958 period. The most significant of these were the reports by DeGraaf and Van Der Held [13] and by Robinson and Powlitch [37] in Housing Report 32 of the Housing and Home Finance Agency, 1954.

DeGraaf and Van Der Held conducted an experimental study of the convection phenomena in plane air layers. In their tests, they measured the heat transferred to the cold surface cooling fluid and based the calculation of the average Nusselt number on this value. Measurements of the average Nusselt number were made at 10 degree increments

in the enclosure inclination with respect to the gravity vector from the horizontal (bottom surface heated) to the vertical. The result was a Nusselt number-Grashof number correlation for each discrete angle.

Experiments were carried out for only the horizontal, 45 degrees, and vertical inclination in Housing Report 32 but provided data for very large enclosures. The work was undertaken to predict heat losses in the home construction industry and the correlations were later converted by Tabor for use in solar collector design.

Dropkin and Somerscales [15] conducted an experimental study of natural convection of liquids confined by two parallel plates and inclined at various angles, and Globe and Dropkin [20] conducted a similar study for the horizontal orientation. The fluids investigated were water, mercury and 2 and 1000 centistoke oil. These fluids provided a range of Prandtl numbers between .02 and 11560 and enabled the authors to determine Prandtl number effects on Nusselt number. The resulting form of the correlations is:

$$\overline{Nu}_L = C(Ra_L)^{1/3} (Pr)^{.074}$$

where $\overline{Nu}_L$ is the Nusselt number, Ra_L is the Rayleigh number, Pr is the Prandtl number, and C is a constant varying from .069 for the horizontal to .049 for the vertical. The results of Dropkin and Somerscales for the horizontal orientation agreed with those of Globe and Dropkin, even though the latter used a circular test section. The test apparatus of Dropkin and Somerscales was similar to that of DeGraaf and Van Der Held with the difference of the two being in the measurement of the heat flow. Dropkin and Somerscales measured the electrical input to the

heater and used this in the calculation of Nusselt numbers.

Boundary layer theory suggests a correlation in which the exponent on Grashof or Rayleigh number is 1/4 for laminar flow and 1/3 for turbulent flow. Dropkin and Somerscales, in their research, assumed for all inclinations that the flow was everywhere turbulent as evidenced by the exponent of 1/3 on the Rayleigh number in their correlation. Macgregor and Emery [30] question whether the assumption of turbulent flow postulated by Dropkin and Sommerscales actually existed in the range of Grashof numbers less than 10^6. DeGraaf and Van Der Held report that Nusselt number is a function of $Gr_L^{.4}$ for low Grashof numbers and $Gr_L^{.37}$ for large Grashof numbers at all inclinations; whereas, Catton and Edwards [8] suggest that the exponent should never exceed .29 for the horizontal orientation.

The post-1970 period saw rapid advances in both the experimental and theoretical development of free convection in inclined air layers. The bulk of experimental work has been undertaken by Hollands et al., [24,25,26,34,35,36] at the University of Waterloo and by Catton et al., [1,2,3,6,8,9,10,11] at UCLA. The work done at UCLA has been mainly involved in low to moderate aspect ratio enclosures ($H/L < 15$).

Raithby and Hollands [34,35] formulated a general model which was later used in subsequent experimental investigations as a basis for predicting heat transfer rates. This model assumes that the major resistance to heat flow occurs in the boundary layers along the hot and cold plates, represented by an equivalent conduction layer thickness

(a thickness of stagnant fluid offering the same resistance to flow as the boundary layer), while in the center the mechanism is by conduction alone. The resulting equations are analagous to those of condensation on an isothermal surface.

The validity of this model was later checked by Hollands, Raithby, and Konicek [25] in a study of free convection in horizontal layers of air and water. The experimental setup at the University of Waterloo is worthy of mention because it represents another method of varying Rayleigh number rather than the conventional method of changing plate spacing and/or temperature difference. It consists of a 1/2 inch by 25 inch air space maintained at a constant 10 degrees centigrade temperature difference. The heat transfer is measured only in the central five inches of the test section through the use of a heater-guard heater arrangement. Inherent in this measurement is the assumption that the flow in the central region is fully developed and that the end turn-around regions do not contribute significantly to the total heat transfer. The apparatus is then placed into a pressure vessel and Rayleigh number is varied by varying the vessel pressure. This study yielded results which agreed quite well with the model for the horizontal position.

Based upon Hart's observation that the instability associated with inclined air layers of tilt angles less than 72 degrees is the same instability associated with the horizontal Benard convection, Clever [12] theoretically investigated the possibility that the Nusselt number at any tilt angle can be scaled from the horizontal simply by replacing the acceleration of gravity, g, in Rayleigh number by $g\cos(\phi)$,

where ϕ is the collector tilt angle.

$$\overline{Nu}_L(\phi, Ra_L) = \overline{Nu}_L(\phi=0, Ra_L COS(\phi))$$

He showed that for an infinite Prandtl number fluid and very large aspect ratios this substitution is valid and used Dropkin and Somerscales' and DeGraaf and Van Der Held's data to confirm his conclusions. Buchberg, Catton, and Edwards [6] suggested that these results are actually valid for low Prandtl number fluids in enclosures of aspect ratio larger than 10. Arnold, Catton, and Edwards [1] examined experimentally the effect of replacing g by gCOS (ϕ) for inclined layers and found good agreement provided the aspect ratio is greater than three.

The conclusion that g can be replaced by gCOS (ϕ) in the Rayleigh number represented a major breakthrough in free convection correlations for inclined plane layers. Hollands et al., [26] re-examined Clever's result and were able to justify relaxing the Prandtl number restriction. The authors then investigated heat transfer in tilted cavities using the same apparatus from [25] and compared the results for the tilted cavity to the results from the horizontal using the cosine phi scaling. Excellent agreement was noted for angles up to 15 degrees; but, for larger angles a departure from prediction was observed. No explanation is available for these deviations and an empirical modification was made to the derived equations to obtain a better fit of the data. The resulting equation is:

$$\overline{Nu}_L = 1.+1.44\left[1.-\frac{1708}{Ra_L COS(\phi)}\right]\left(1.-\frac{SIN(1.8\phi)^{1.6}1708}{Ra_L COS(\phi)}\right) + \left[\left(\frac{Ra_L COS(\phi)}{5830}\right)^{1/3} -1.\right]$$

Valid for $\phi < 60$

where $[X]^{\cdot} = \frac{X + [X]}{2}$

The above equation was found to fit the experimental data to ±5% over the valid range of tilt angles. Agreement is found to be ±10% at 70 degrees inclination.

1.2.3 Vertical Flat Plate Enclosures

Attempts to arrive at accurate correlations for tilt angles greater than the roll cross-over angle (72°-78°) have not been fruitful. This is a consequence of the fact that at large tilt angles the flow reversals along the end spacers are much more severe and an aspect ratio dependency is expected, particularly at smaller aspect ratios where the reversals occupy a greater percentage of the area. As a result, it is imperative that the thermal boundary condition be known in any experimental set-up used to investigate tilt angles near vertical.

For vertical flat plates, the functional relationship between the local Nusselt number for the hot or cold surface and the other parameters is of the form:

$$Nu_x = f(Gr,Pr,H/L,W/L,x/L)$$

where H is the height of the air layer, W is the width of the air layer, L is the thickness of the layer, and x is the distance along the plate. Most authors agree that the width to thickness ratio has little or no effect on the Nusselt number and that the Prandtl number of air remains relatively constant. By far, the biggest disparity between authors occurs in the determination of the effect of the height to thickness ratio (Aspect ratio) on Nusselt number.

Dropkin and Somerscales varied the aspect ratio for their test

section between 4.41 and 16.56 and determined that there is no significant affect on Nusselt number due to this variation. DeGraf and Van Der Held also arrived at the same conclusion for all inclinations.

An interferometric investigation of two parallel vertical plates [7,17] obtained similar results to those of Brooks and Probert [5]. Eckert and Carlson measured the hot surface heat flux and used this to calculate a Nusselt. The authors found that there is an affect of aspect ratio on Nusselt number which contradicts the results of [13,15].

Some authors have found a definite affect of aspect ratio on the Nusselt number [7,17,18,30,36] for the vertical. However, there is not good agreement on what the magnitude of the exponent on aspect ratio should be. The reported range of exponents is from -1/10 [17] to -1/3 [30]. From this, it is seen that that the lower the aspect ratio, the greater will be the Nusselt number. The increase of Nusselt number above 1 is a measure of convection effects and flow non-uniformities at the ends of the cell. Batchelor [4] has shown that the height of the end affects in the cell is approximately equal to the width of the cell. Thus, as the aspect ratio is decreased, the end effects occupy a greater percentage of the cell and the Nusselt number would tend to increase. A similar but progressively less predominant affect would be expected as the cavity is rotated to the horizontal.

By making the usual boundary layer assumptions and an order of magnitude analysis on the resulting equations of motion and the energy equation, Ayyaswamy and Catton [3] suggest that the results for the well known vertical cavity can be scaled to tilt angles of less than 90 degrees. The constraints imposed upon the results are:

1) the flow is in the laminar boundary layer regime, (2)$Ra_L SIN(\phi) \geq 1000$, and (3) the tilt angle is between 70 degrees and 150 degrees (top surface heated). The results compare to those of (10) to within ± 4%. The resulting equation is:

$$\overline{Nu}_L(\phi) = \overline{Nu}_L(\phi=90°)SIN(\phi)^{1/4} \qquad 70 \leq \phi \leq 150$$

Raithby, Hollands, and Unny [36] have also undertaken a theoretical investigation for the prediction of heat transfer in vertical enclosures bounded by vertical differentially heated isothermal walls and adiabatic top and bottom surfaces. This yielded equations for the mid-core temperature distribution for the laminar and turbulent boundary layer regimes. The resulting temperature profiles agree well with those of [7,17]. The Nusselt number-Rayleigh number correlations that were derived for the vertical layer are:

$$\overline{Nu}_L = [1., .75\ C_l\ A^{1/4} Ra_L^{1/4}, .29\ C_t\ Ra_L^{1/3}]_{MAX}$$

where C_l and C_t are functions of Prandtl number only and MAX indicates that the maximum of the values in brackets is applicable. The terms in brackets represent the conduction, laminar boundary layer, and turbulent regimes, respectively. The authors suggest, without verification, that Ra_L can be replaced by $Ra_L SIN(\phi)$ for $70 \leq \phi \leq 150$.

2. *EXPERIMENTAL APPARATUS*

Figure 1 shows a schematic of the experimental apparatus used in the investigation. It was designed to provide a two-dimensional

flow pattern parallel to the glass plates and to have isothermal surfaces. The lower surface consists of an 18"x4"x1/2" copper plate while the upper, of the same size, is constructed of aluminum. The copper plate is electrically heated by a flat foil-type heater cemented to the back and the aluminum plate is cooled by water passing through channels machined into the backside. Surface temperature measurements are obtained from nine thermocouples penetrating each plate from the rear to the front face. Maximum temperature deviations of 1°F over the surface of the cold plate and less than 3 F over the surface of the hot were observed at a temperature differences up to 160°F. Each surface was polished and nickel plated to reduce radiation contributions to the total heat flow for energy balance purposes, although the interferometric technique is not sensitive to radiation heat transfer.

Because of the small diameter of the interferometer light beam (3 inches) it was necessary to devise a method of moving the test section relative to the light path in order to view the entire enclosure length. A rigid channel consisting of bakelite sides and surrounded by 2 inches of styrofoam insulation was constructed and into which the test section fit snugly. Two flat-glass windows were inserted into opposite sides of the channel so that the interferometer light beam could pass through the air layer. The test apparatus could then slide past the windows so the air layer could be viewed through the interferometer in its whole extent while the bakelite channel provided lateral retaining walls for the air layer. A number of tests were performed to determine the time required for the temperature profiles of the air layer to reach steady-state after the test apparatus had been moved to a new viewing station (usually at 1 inch intervals). It

was found that a steady-state is established within a thirty-minute time period and that pictures could be accurately taken after 40 minutes following movement of the test section.

The aspect ratio of the air layer was varied using interchangeable end spacers. These spacers are constructed of a laminated insulation material similar to bakelite. Accurate measurements of the temperature profile along the surface with the interferometer showed it to be very close to linear.

Figure 2 presents a summary of the Aspect ratio-Grashof Number-tilt angle ranges examined in this study. In all cases the plate length is 18 inches with the sole exception of A=9. In this case a false spacer was placed in the middle of the enclosure. The ranges are limited by the maximum temperature capability of the thermocouples, the minimum temperature difference and minimum plate spacing at which accurate measurements can be made, and the maximum viewable plate spacing.

The Mach-Zehnder interferometer is used to measure the temperature profiles, which, in turn, are used to evaluate the local heat-transfer rates. This is the same instrument designed and constructed by Ross [38]. The interferometer measures the integrated average of the index of refraction in the light path direction relative to some reference point (in this case the cold surface). There are equations available which relate index of refraction differences to density differences [21], (the well known Gladstone-Dale Equation, for example), and the changes in optical path length to the temperature differences for uniform pressure conditions. The localized fringe patterns were photographed for analysis.

Interferograms were examined on an optical comparator to determine the temperature at discrete intervals across the air layer. Near the surface the temperature points were fitted numerically to a polynomial using a least squares routine. With the temperature profiles thus obtained, the temperature gradients at the wall were obtained by differentiation. The foregoing steps were repeated at each axial position where the local Nusselt number was desired.

From the equation

$$q'' = -K_w \left.\frac{\partial T}{\partial y}\right)_w = h\,(T_H - T_C) \tag{1}$$

which defines the local heat transfer coefficient at the hot or cold surface, the following relation

$$Nu_w \doteq \frac{hL}{K} = -\left.\frac{\partial \Theta}{\partial \bar{y}}\right)_w \tag{2}$$

is obtained for the local Nusselt number based upon the plate spacing, L, and with the thermal conductivity evaluated at the wall temperature. Nu_w can also be interpreted as the ratio of an apparent local thermal conductivity of the air layer to the actual conductivity. However, in order to be consistent with the reported literature, the local Nusselt number based upon the mean temperature of the hot and cold surface is desirable. The mean Nusselt number then becomes the non-dimensional temperature gradient at the surface multiplied by the ratio of the thermal conductivity evaluated at the surface temperature to the thermal conductivity evaluated at the mean enclosure temperature

$$Nu_L = -\frac{K_w}{K_m}\left.\frac{\partial \Theta}{\partial \bar{y}}\right)_w \tag{3}$$

All transport quantities reported hereafter are evaluated at the mean enclosure temperature. The average Nusselt number is found by numerically integrating the local values over the entire plate length

$$\overline{Nu}_L = \frac{\overline{h}L}{K} = \frac{1}{H}\int_0^H Nu_L dx \tag{4}$$

The use of interferometry for the measurement of heat-transfer coefficients presents certain advantages over conventional methods. The most important is that it permits accurate determination of local temperature profiles and heat fluxes without physically interfering with the flow field. It also gives information on the flow field simultaneously over a fairly extended region and is completely free of inertia (and this is particularly important when analyzing regions which contain marginally unstable flows). Since the interferometer detects only density differences, the results require no correction for radiation contributions to the convective heat transport provided that the medium is non-participating in the radiative transport.

However, the use of interferometry and the 3" U.W. interferometer restricts the size and orientation of enclosures that can be analyzed. As previously mentioned, the index of refraction, and therefore density, is integrated along the light path. This presents no special problems in disturbances which are two-dimensional or axisymmetric but makes analysis of three-dimensional disturbances difficult. It was not possible to accurately analyze horizontal air layers in which highly three-dimensional Benard convection

cells occur. An attempt was made using time lapse photography and averaging of the resulting Nusselt numbers; however, they fell consistently and considerably below the values reported in the literature. Other physical restrictions imposed upon the system were:

(1) The choice of a 4" width of the cell in order to minimize refraction effects. Refraction of the light beam occurs in traversing a disturbance in which there are transverse index of refraction gradients. These can be significant in cells of large width [21].

(2) Enclosure tilt angles less than 33° from the horizontal could not be studied due to physical interference of the test apparatus with the reference beam of the interferometer.

(3) Plate spacings were limited due to the 2" x 3" eliptical shape of the interferometer field of view. This constraint also puts an upper limit on Grashof number of about 3×10^5.

3. *HEAT TRANSFER RESULTS*

3.1 *Conduction Regime*

Heat transfer in the conduction regime is traditionally characterized by purely molecular conduction in the center of the enclosure. In this region, $Nu_L = 1$. It is known that there is a net fluid motion as evidenced by the convective transport in the end turn-around

regions where $Nu_L \neq 1$. Analysis of interferograms for this case shows that there is, in fact, a boundary layer which develops on each surface and merges quite rapidly. In the boundary layer, there is no net convection in the center section of the cavity.

In the lower corner of the hot plate and the upper corner of the cold plate (termed the starting corners by Eckert and Carlson [17]) the local heat transfer coefficient is larger than the average by a factor of at least two. In the upper corner of the hot plate and lower corner of cold plate (termed the departure corners) it is lower. As would be expected of cavity flows in which there are not significant differences in temperature between the hot and cold surfaces, there is unicellular flow (termed the base flow by Hollands et al. [26]) and the flow is assymetric about the cavity midpoint. In this case the local Nusselt number profiles along the hot and cold plates are the same with respect to the starting corner.

For large Aspect Ratio enclosures the end turnaround regions do not occupy a large portion of the enclosure, i.e. they do not penetrate to the center. In this case one would expect the local heat transfer in the ends to be a function only of the plate spacing, L, and independent of the plate lengths, H. Eckert and Carlson [17] have investigated the vertical orientation with the interferometer and found the relation for local Nusselt numbers in the corners to be

$$Nu_x = f(Gr_x, X/L).$$

They have found the relation for the local heat transfer in the starting corners to be

$$Nu_{x,s} = .256\ Gr_x^{.24} \qquad \phi = 90° \tag{5}$$

and for the departure corners to be

$$Nu_{x,d} = 2.58\ Gr_x^{.4}\ (Gr_L)^{-.55} \qquad \phi = 90° \tag{6}$$

where x is the distance measured from the respective corners.

We have chosen to parallel the Eckert and Carlson study while extending the results to other collector tilt angles. Figure 3 shows a representative plot of local Nusselt number versus non-dimensional plate length for $\phi = 60°$ and $Gr_L = 4000$. As shown by Hollands and Konicek [24] this value of Gr_L is below the critical Grashof number for this angle of inclination. It is evident that there is a significant departure from conduction in the starting corner while the departure corner has a mild deviation from conduction. The location of the maximum and minimum in the starting and departure corners, respectively, is a consequence of the boundary conditions imposed upon the spacers. The linear temperature profile forces the Nusselt number to approach one as x goes to 0. As a result there are very sharp gradients in the local Nusselt profiles near the spacers and these have been neglected in determining correlations for local Nusselt numbers, Nu_x, as a function of distance from the corners.

The resulting correlations for heat transfer in the starting corners are:

$$Nu_{x,s} = .30\ Gr_x^{0.21} \qquad \phi = 75° \tag{7}$$

$$Nu_{x,s} = .30\ Gr_x^{0.21} \qquad \phi = 60° \tag{8}$$

$$Nu_{x,s} = .26\ Gr_x^{0.21} \qquad \phi = 45° \tag{9}$$

The above equations present a method of determining the magnitude of the end effects in the starting corner for the conduction regime. The heat transfer coefficient decreases monotonically until it reaches a point where the local Nusselt number equals unity. This point is called the penetration depth, x_p. Eckert and Carlson present a detailed procedure for finding the penetration depth and the average heat transfer in the corner. The penetration depth expressed as the ratio of the penetration depth to the plate spacings and the average Nusselt numbers in the starting corners are given by the following relations

$$X_{p,s}/L = 0.043\ Gr_L^{0.54} \qquad \overline{Nu}_{L,s} = 1.62 \qquad \phi = 75° \tag{8}$$

$$X_{p,s}/L = 0.043\ Gr_L^{0.54} \qquad \overline{Nu}_{L,s} = 1.62 \qquad \phi = 60° \tag{9}$$

$$X_{p,s}/L = 0.031\ Gr_L^{0.54} \qquad \overline{Nu}_{L,s} = 1.62 \qquad \phi = 45° \tag{10}$$

The heat transfer rate in the departure corner was found to be a function of the plate spacing. Eckert and Carlson found the parameter which includes the plate spacing and adequately describes the heat transfer to be Gr_L. They arrived at the following correlation for $Nu_{x,d}$

$$Nu_{x,d} = 2.58\ Gr_x^{.4}\ Gr_L^{-.55} \qquad \phi = 90° \tag{11}$$

where x is now measured from the departure corner. They also found the departure distance and average Nusselt number to be

$$X_{p,d}/L = .00875\ Gr_L^{.75} \qquad \phi = 90° \tag{12}$$

$$\overline{Nu}_{L,d} = .835$$

Again, the same form of equations was chosen to correlate the present results for other tilt angles. The following equations were found to fit the data

$$Nu_{x,d} = 2.85\ Gr_x^{.4}\ Gr_L^{-.55}$$
$$X_{p,d}/L = .0051\ Gr_L^{.75} \qquad \phi = 45° \qquad (13)$$
$$\overline{Nu}_{L,d} = .833$$

$$Nu_{x,d} = 3.2\ Gr_x^{.38}\ Gr_L^{-.55}$$
$$X_{p,d}/L = .003\ Gr_L^{.75} \qquad \phi = 60° \qquad (14)$$
$$\overline{Nu}_{L,d} = .834$$

$$Nu_{x,d} = 3.27\ Gr_x^{.4}\ Gr_L^{-.55}$$
$$X_{p,d}/L = .0027\ Gr_L^{.75} \qquad \phi = 45° \qquad (15)$$
$$\overline{Nu}_{L,d} = .835$$

From the above it can be seen that the penetration depth in the departure corner for a vertical enclosure is substantially larger than that for inclined enclosures

The computation of heat transfer rates in the conduction regime is a special case because the Nusselt number in the center of the enclosure is known to be unity provided that the end turnaround regions do not penetrate to the center of the cell. The average heat transfer coefficient along the plate surface is given by

$$\bar{h} = \frac{1}{H}\left[\bar{h}_s X_{p,s} + \bar{h}_c(H-X_{p,s}-X_{p,d}) + \bar{h}_d X_{p,d}\right] \tag{16}$$

or defined in terms of Nusselt numbers.

$$\overline{Nu}_L = 1 + (\overline{Nu}_{L,s}-1)X_{p,s}/H + (\overline{Nu}_{L,d}-1)X_{p,d}/H \tag{17}$$

Equations (5) thru (15) can be substituted into (17) to determine the average heat transfer rate for a given collector in the conduction regime.

3.2 *Laminar Boundary Layer Regime*

When the Grashof number is increased beyond the critical value, the base flow becomes unstable and buoyancy driven laminar boundary layers form on the hot and cold surfaces. For small Grashof numbers the thermal boundary layers build up in a manner similar to flow over vertical heated and cooled flat plates in an infinite medium. The boundary layers are relatively thick and merge together in the center of the cavity. An analysis of interferograms taken under these conditions shows that the major portion of the heat transfer occurs in the boundary layer by convection while in the center a small portion is transferred by conduction. This phenomena of the boundary layer regime is generally referred to as the transition region or the assymptotic boundary layer region. The local Nusselt number profile, Nu_L, is characteristically a continuously decreasing function of distance along the plate as shown by aspect ratios (A) of 12 and 14.4 in Figure 4.

A further increase in Grashof number results in the formation

of individual laminar boundary layers on the hot and cold surfaces separated by a region which is thoroughly mixed by eddy diffusion. Continuous observations of the temperature profiles shows that the fluid in the boundary layer flows in laminae. In the center, continuous mixing occurs and eddies can be seen to randomly separate from the outer edges of the laminae and disappear into the core. This mixing effect results in large scale perturbations of the temperature profiles near the boundary. The temperature profile across the cavity therefore varies significantly with time. Eckert and Carlson also noted the fluctuations of the temperature in the core and the low frequency fluctuations of the temperature profiles in the boundary layer when the Nusselt profile flattened out [17]. They termed these fluctuations as turbulent, but, they are large relative to the width of the cavity and should more correctly be called unsteady.

Figure 5 shows four interferograms taken in the center of the enclosure for a tilt angle of 75°, a plate spacing of .75", and a Grashof number of 26000 These pictures were taken at different times to show the effect that eddy diffusion in the core has on the cavity temperature distribution. An analysis of free convection under these conditions requires multiple pictures to obtain a time averaged local Nusselt number. The local Nusselt profiles for heat transfer in this unsteady region of the laminar boundary layer regime show a flattening, or plateau, in the center of the enclosure where eddy effects occur. Figures 6 and 7 show characteristic profiles. The actual data points are shown on the figures demonstrating the wide

fluctuations of local Nusselt number in the enclosure center. The constant local Nusselt number in the center of the cavity means that the local wall heat flux is a constant. Therefore, there is no boundary layer buildup here and the main transport mechanism is eddy diffusion across the channel.

3.2.1 Local Heat Transfer

The formation of the boundary layers in the starting corner strongly resembles that which occurs in the flow of air over a vertical heated plate in an infinite medium. This suggests that the local variations of the Nusselt number, Nu_L , can be correlated by

$$Nu_x = C\ Gr_x^n \tag{18}$$

for any given angle, where C and n are constants. The characteristic distance, x, is the distance from the starting corner. A correlation of this form must, however, exclude the region close to end spacer because as for the conduction regime, the local Nusselt profile must fit the temperature profile on the spacer, i.e.

$$Nu_L \Big|_{x=0} = 1$$

The maximum Nu_L , generally occurs within the first half inch of the enclosure. We have found that the characteristic temperature difference used in Grashof number which accurately describes the heat transfer process is (T_H-T_c) whereas Eckert and Carlson found it to be (T_w-T_m) where T_m is the temperature in the centerline of the enclosure at the position x. We have used the temperature difference (T_H-T_c) in our work.

Figure 8 presents the results of a least square analysis of all experiments for angles of 45, 60, 75, and 90 degrees. The range of aspect ratios from 9 to 24 correlates quite well when the properties are evaluated at the mean temperature of the hot and cold plates. Note that both the runs in the transition region and in the region dominated by the eddy diffusion effect correlate equally well into a single line. A least square fit of the data results in the following equations which fit the experiments to within ±5%:

$$\begin{aligned} Nu_x &= .335\ Gr_x^{.222} && \phi = 90° \\ Nu_x &= .292\ Gr_x^{.228} && \phi = 75° \\ Nu_x &= .232\ Gr_x^{.245} && \phi = 60° \\ Nu_x &= .238\ Gr_x^{.245} && \phi = 45° \end{aligned} \qquad (19)$$

Attempts to correlate the local variations of the heat-transfer coefficient in the departure end are complicated by the fact that the flow in this area resembles flow into a stagnation point. As such, there appears to be an effect of plate spacing as well as tilt angle on the results. The experimental results for ϕ = 90 degrees are shown in Figure 9. All test runs using the same plate spacing appear to correlate well regardless of Gr_L and the plate length. The single dominant effect is apparently the plate spacing. This prevents the use of a non-dimensional quantity as the correlating parameter. We are continuing efforts to arrive at accurate correlations for predicting the local heat transfer in the departure corner.

For tilt angles less than 90° the penetration depth in the starting and departure corners becomes progressively smaller as the angle is decreased due to the introduction of the component of the bouyant force perpendicular to the wall. Figure 10 demonstrates the effect of tilt angle on the local profile for an aspect ratio of 18 and a Grashof number of 93000. At angles of 45° and 60° the end effects occupy approximately the same area as evidenced by equation (19) and play less of a role in the total heat transfer. For all runs at 45 and 60 degrees the end effects failed to penetrate to the center of the enclosure for aspect ratios greater than 12. This suggests that the measurements of Holland's et al. [26] in which the heat transferred is measured only in the center of the enclosure is a valid method.

At angles near vertical the disturbance caused by the corners occupies a much larger portion of the enclosure and may in fact occupy the whole area. It is to be expected that any effect of aspect ratio on the total heat transferred would be evident at this angle. Figure 4 shows three aspect ratios for the vertical orientation at a Grashof number of 93,000. It is evident that the lowering of the aspect ratio from 18 to 14.4 and 12 has the effect of forcing the flow into the transition region of the laminar boundary layer regime.

Average Heat Transfer

For all experimental profiles the local Nusselt numbers have been integrated using equ.4 to determine the average. From an examination of the equations of change for this system one would expect the average heat transfer to be of the form

$$\overline{Nu}_L = f(Gr_L, Pr, H/L, W/L, \phi). \qquad (20)$$

The width aspect ratio, W/L, can be neglected if the cavity is large enough in the transverse direction (in the light path direction for this study). An examination of Fig. 4 reveals that the effect of the height aspect ratio (H/L) on the average heat transfer is actually determined by the penetration depth of the disturbances in the starting and departure corners. For very large collectors these disturbances may each occupy a relative small area separated by a region in which Nu_L is essentially constant. As the collector length decreases the disturbances occupy a larger area until the point is reached where the entire enclosure is occupied by end effects. For a fixed plate spacing and Grashof number, the end effects occupy a smaller portion of the collector area as the angle from the horizontal decreases. The largest end effect is in a vertical collector. This is due to the introduction of the component of bouyant force perpendicular to the wall which forces the boundary layers to develop faster. This effect is evident on Figure 10. Where, for the same Grashof number and aspect ratio, the end effects decrease as ϕ decreases.

Equations have previously been presented for computation of average

heat transfer in the conduction regime. These equations and Figure 3 show the aspect ratio effect on the total heat transfer. For the profile shown on Figure 3 the local Nusselt number in the center of the enclosure is approximately one while there is a significant departure from this value at the ends. For experiments in which the heat transfer is measured only in the center 5 inches of the enclosure, $\overline{Nu}_L$ would be measured as equal to 1. For this run, $\overline{Nu}_L$ evaluated over the entire 18 inch plate length is 1.06 a difference of +6%. If the plate length is longer, then the penetration depth is the same and $\overline{Nu}_L$, found by integrating over the length, approaches 1.

Heat transfer in the boundary layer regime is complicated by the fact that there are two distinct flow patterns: one in which the boundary layers join together and one in which the boundary layers are separated by a mixed core. In the case of the separated boundary layers $\overline{Nu}_L$ is accurately reflected in the local Nusselt numbers in the center of the cavity. This is not so when the boundary layers have joined. However, while there is definitely an aspect ratio effect on the local profile due to the different boundary layer structure, the integrated average Nusselt number does not show any significant aspect ratio effect for the range of aspect ratios examined in this study. In all runs in which there is an effect on the local profiles, $\overline{Nu}_L$ for the smaller a exceeds that for the larger in the starting corner, while in the departure corner, the value for the higher A exceeds that for the smaller. The net effect is to bring the averages into close agreement. An effect of aspect ratio of the magnitude predicted by [17] and [18] was not noted.

Figures 11 and 12 present a comparison of these results with correlations of past reports which have found no aspect ratio dependency for tilt angles of 45 and 90 degrees respectively. In general the results fall midway between the correlations. Figure 13 compares these results with the correlation of Hollands et al., the correlation for 45° is also shown; however, the 60° curve falls virtually on top of the 45° curve. The present results fall somewhat below the curve but follow the same general trend. The data points at the lower end fall above the correlation because of the effect of aspect ratio in the conduction regime described earlier.

Reference [36] suggests that the results in the well studied vertical cavity can be scaled to angles as low as 70°. The suggested correlation is

$$Nu_L = [1,\ .75\ C_\ell A^{-1/4}(Ra_L \sin\phi)^{-1/4},\ .29C_t(Ra_L \sin\phi)^{1/3}]_{MAX} \qquad (21)$$

where

$$C_\ell = .50/[1+(.49/Pr)^{9/16}]^{4/9} \text{ and } C_t = [.14Pr^{.084},\ .15]_{MIN}$$

Figure 14 shows this correlation for $\overline{Nu}_L$, the correlation of [13] and [32], and some results from this study plotted versus tilt angle. Equ. 21 predicts $\overline{Nu}_L$ to be an increasing function of tilt angle while this study and the results of [13] and [32] predict $\overline{Nu}_L$ to be a decreasing function of tilt angle.

This observation suggests the possibility of scaling the results of $\phi = 45°$ to larger angles. We attempted to correlate the data as Nu_L vs. $Ra_L \cos(\phi=45°)$. However this failed to pull the results for various tilt angles together. We found that a plot of Nu_L vs. $Ra_L \cos^2(\phi-45°)$

resulted in a good correlation. The data, correlated on this basis, is shown on Figure 14. A lease square fit of the data results in a correlation of the form

$$Nu_L = .118[Ra_L \cos^2(\phi-45°)]^{.29} \quad 45° \leq \phi \leq 90° \qquad (22)$$

which fits the data to $\pm$ 8%. This provides a correlation which is continuous over a range of tilt angles from 45° to 90°.

The designer interested in determining the magnitude of end effects for flow in the separated boundary layer regime now has some of the tools necessary to do this. When an estimate of the local variations of the heat transfer coefficient in the separated boundary layer regime is desired,

(1) using equ (22) or the correlation of one of the referenced authors to determine $\overline{Nu}_L$ in the center of the plate.

(2) using equ's. (19) to generate the local profile in the starting corner and extending this until it meets the center value from step 1.

(3) using an as yet to be developed equation for predicting the local profile in the departure corner.

will generate a typical local $\overline{Nu}_L$ profile.
Work is also progressing on a method of determining local profiles for flow in the transition region.

The experimental results for the average heat transfer are given in Table 1.

TABLE 1

EXPERIMENTAL RESULTS

Enclosure Angle	Aspect Ratio	Grashof Number, Gr_L	Average Nusselt Number, $\overline{Nu}_L$
90°	24	36000	1.95
		16000	1.43
		9600	1.12
	18	37000	1.84
		9000	2.51
	14.4	210000	3.14
		91000	2.50
		35600	1.85
	12	98000	2.50
		210000	2.93
75°	36	4230	1.09
	18	92500	2.72
	12	225000	3.17
	9	85000	2.65
60°	36	4000	1.06
	18	93000	2.91
	12	210000	3.40
	9	93000	2.82
45°	36	4000	1.10
	18	54700	2.76
		93000	3.06
	14.4	33000	2.49
	10.3	370000	4.44
	9	90000	2.95

4. *BIBLIOGRAPHY*

1. Arnold, J. N., I. Catton, and D. K. Edwards, "Experimental Investigation of Natural Convection in Inclined Rectangular Regions of Differing Aspect Ratios," J. Heat Transfer, Vol. 1976, pp. 67-71.

2. Arnold, J. N., D. K. Edwards, and I. Catton, "Effect of Tilt and Horizontal Aspect Ratio on Natural Convection in Rectangular Honeycomb Solar Collectors," ASME Paper 76-HT-18.

3. Ayyaswamy, P. and Catton, I., "The Boundary Layer Regime for Natural Convection in a Differentially Heated, Tilted Rectangular Cavity," J. Heat Transfer, Trans. ASME, Vol. , 1973, pp. 543-545.

4. Batchelor, G. K., "Heat Transfer by Free Convection Across a Closed Cavity Between Vertical Boundaries at Different Temperatures," Quart. Applied Math., Vol. 12, 1954, pp. 209-233.

5. Brooks, R. C. and S. D. Probert, "Heat Transfer Between Parallel Walls: An Interferometric Investigation," J. Mech. Eng. Sci., Vol. 14, No. 2, 1972.

6. Buchberg, H., I. Catton, and D. K. Edwards, "Natural Convection in Enclosed Spaces: A Review of Application to Solar Energy Collection," ASME Paper 74-WA/HT-12, 1974.

7. Carlson, W. O., PhD Thesis, University of Minnesota, 1956.

8. Catton, I., and D. K. Edwards, "Effect of Side Walls on Natural Convection Between Horizontal Plates Heated from Below," J. Heat Transfer, Vol. 89, 1967, pp. 295.

9. Catton, I., "Convection in a Closed Rectangular Region: The Onset of Motion," J. Heat Transfer, Trans. ASME, Vol. 94, 1972, pp. 186-187.

10. Catton, I., P. Ayyaswamy, and R. M. Clever, "Natural Convection Flow in a Finite Rectangular Slot Arbitrarily Oriented with Respect to the Gravity Vector," Int. J. Heat Mass Transfer, Vol. 17, 1974, pp. 173-184.

11. Catton, I., "Effect of Wall Conduction on the Stability of a Fluid in a Rectangular Region Heated from Below," J. Heat Transfer, Vol. 94, 1972, pp. 446.

12. Clever, R. M., "Finite Amplitude Longitudinal Convection Rolls in an Inclined Layer," J. Heat Transfer, Trans. ASME, Vol. 95, 1973, pp. 407-408.

13. DeGraaf, J. and E. Van Der Held, "The Relation Between the Heat Transfer and the Convection Phenomena in Enclosed Plane Air Layers," Appl. Sci. Res., Section A, Vol. 3, 1952, pp. 393.

14. Dixon, M. and S. D. Probert, "Heat-Transfer Regimes in Vertical, Plane-Walled, Air-Filled Cavities," Int. J. Heat Mass Transfer, Vol. 18, pp. 709.

15. Dropkin, D. and E. Somerscales, "Heat Transfer by Natural Convection in Liquids Confined by Two Parallel Plates Which are Inclined at Various Angles with Respect to the Horizontal," J Heat Transfer, Trans. ASME, Vol. 87, 1965, pp. 77-84.

16. Duffie, J. A. and W. A. Beckman, Solar Energy Thermal Processes, New York, John Wiley and Sons, 1974.

17. Eckert, E. R. C. and W. O. Carlson, "Natural Convection in an Air Layer Enclosed Between Two Vertical Plates with Different Temperatures," Int. J. Heat Mass Transfer, Vol. 2, 1961, pp. 106-120.

18. Emery, A. and N. C. Chu, "Heat Transfer Across Vertical Layers," J. Heat Transfer, Trans. ASME, Vol. 91, 1969, p. 391.

19. Farhadich, R. and R. S. Tankin, "Interferometric Study of Two-Dimensional Benard Convection Cells," J.Fluid Mech, Vol 66, 1974, p. 739.

20. Globe, S. and D. Dropking, "Natural Convection Heat Transfer in Liquids Confined by Two Horizontal Plates and Heated from Below," J. Heat Transfer, Trans. ASME, Vol. 81, 1959, p. 24.

21. Hardel, G., PhD Thesis, University of Wisconsin, 19

22. Hart, J. E., "Stability of the Flow in a Differentially Heated Inclined Box," J. Fluid Mech, Vol 47, 1971, pp. 547-576.

23. Hart, J. E., "Experiments with Two-dimensional, Rectilinear, Convective Rolls at Supercritical Conditions," Phy. of Fluids, Vol 15, 1972, p. 203.

24. Hollands, K.G.T. and L. Konicek, "Experimental Study of the Stability of Differentially Heated Inclined Air Layers," Int. J. Heat Mass Transfer, Vol 16, 1973, pp. 1467-1476.

25. Hollands, K.G.T., G.D. Raithby, and L. Konicek, "Correlation Equations for Free Convection Heat Transfer in Horizontal Layers of Air and Water," (submitted for publication).

26. Hollands, K.G.T., T. E, Unny, G. Raithby, and L. Konicek, "Free Convection Heat Transfer Across Inclined Air Layers," J. Heat Transfer, Trans. ASME, Vol 98, 1976, pp.189-193.

27. Hottel, H.C. and B. B. Woertz, "The Performance of Flat Plate Solar Heat Collectors," Trans. ASME, Vol 64, 1942, pp. 91-104.

28. Kantorovich and Krylov, Approximate Methods of Higher Analysis, New York,,Interscience Publishers, Inc. - New York.

29. Kurzweg, U. H., "Stability of Natural Convection Within an Inclined Channel," J. Heat Transfer, Trans. ASME, Vol 8, 1970, pp. 190-191.

30. MacGregor, R. K. and A. F. Emergy, "Free Convection Through Vertical Plane Layers-Moderate and High Prandtl Number Fluids," J. Heat Transfer, Trans. ASME, Vol 91, 1969, p. 391.

31. Norden, P. A. and Usmanov, A. G., "The Inception of Convection in Horizontal Fluid Layers," Heat Transfer-Soviet Research, Vol 4, 1972, pp. 155-161.

32. Ozoe, H. and H. Sayama, "Natural Convection in an Inclined Square Channel," Int. J. Heat Mass Transfer, Vol. 17, 1974, pp. 401-406.

33. Quon, C., "Numerical Studies of Diffusively Induced Convection in a Tilted Square Cavity," ASME paper 76-HT-47.

34. Raithby, G. D. and K.G.T. Hollands, "A General Method of Obtaining Approximate Solutions to Laminar and Turbulent Free Convection Problems," Advanced in Heat Transfer, Vol. 11, Academic Press, 1974.

35. Raithby, G. D. and K.G.T. Hollands, "Laminar and Turbulent Heat Transfer by Natural Convection," Int. J. Heat Mass Transfer, Vol. 17, 1974, pp. 1620-1622.

36. Raithby, G. D., K.G.T. Hollands, and T. E. Unny, "Free Convection Heat Transfer Across Fluid Layers of Large Aspect Ratio," ASME Paper 76-HT-37.

37. Robinson and Powlitch, "The Thermal Insultaion Value of Airspaces," Housing Research Paper 32, Housing and Home Finance Agency, Washington, D.C., 1954.

38. Ross, P. A., PhD Thesis, University of Wisconsin, 1962.

39. Sernas, V., L. S. Fletcher, and C. Rago, "An Interferometric Study of Natural Convection in Rectangular Enclosures of Aspect Ratio Less Than One," ASME Paper 75-Ht-63, 1975.

40. Tabor, H., "Radiation, Convection, and Conduction Coefficients in Solar Collectors," Bull. Res. Council of Israel, Vol. 6C, 1958.

41. Unny, T. E., "Thermal Instability in Differentially Heated Inclined Fluid Layers," J. Applied Mech., 1972, p. 41.

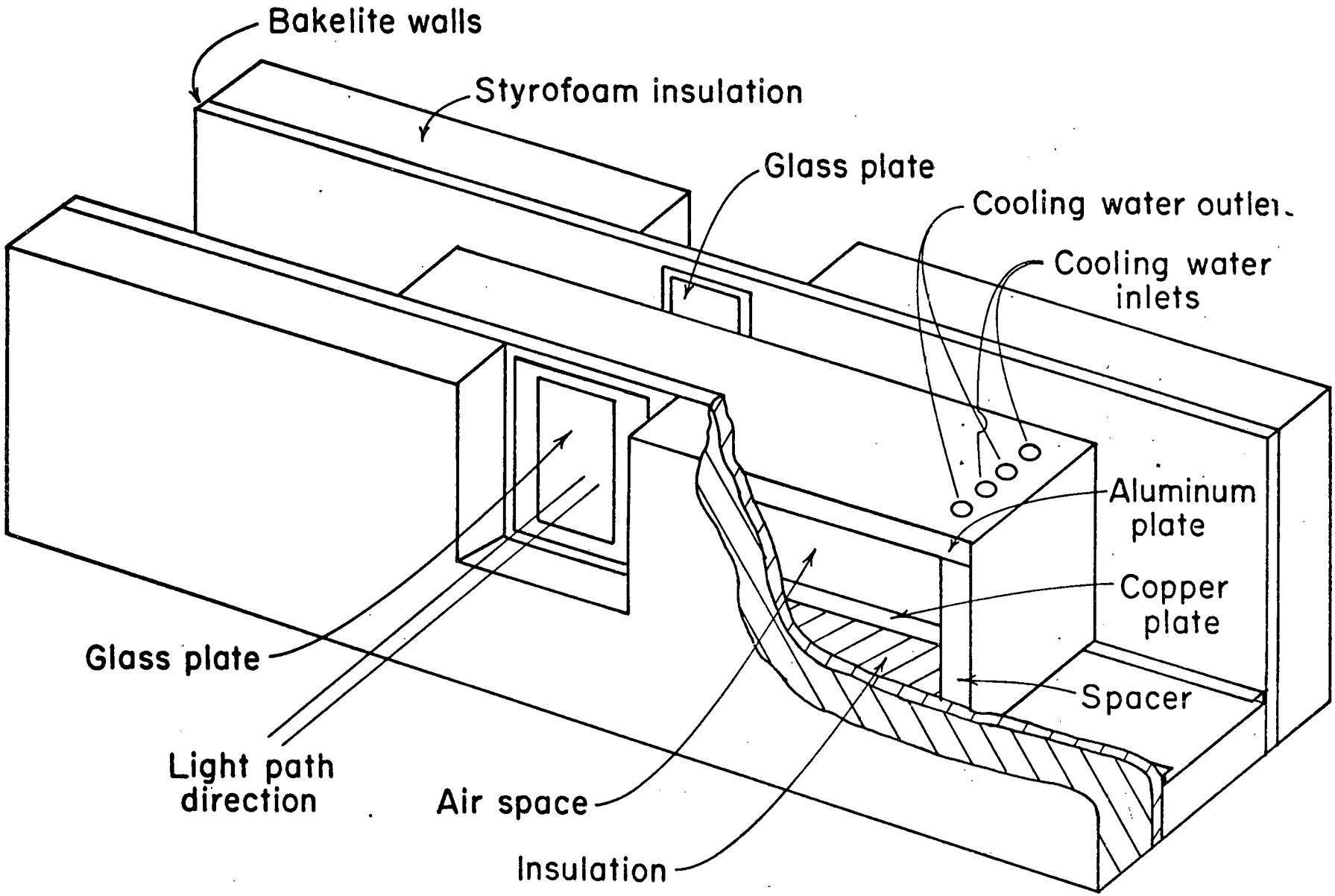
Bakelite walls
Styrofoam insulation
Glass plate
Cooling water outlet
Cooling water inlets
Aluminum plate
Copper plate
Spacer
Glass plate
Light path direction
Air space
Insulation

Figure 1

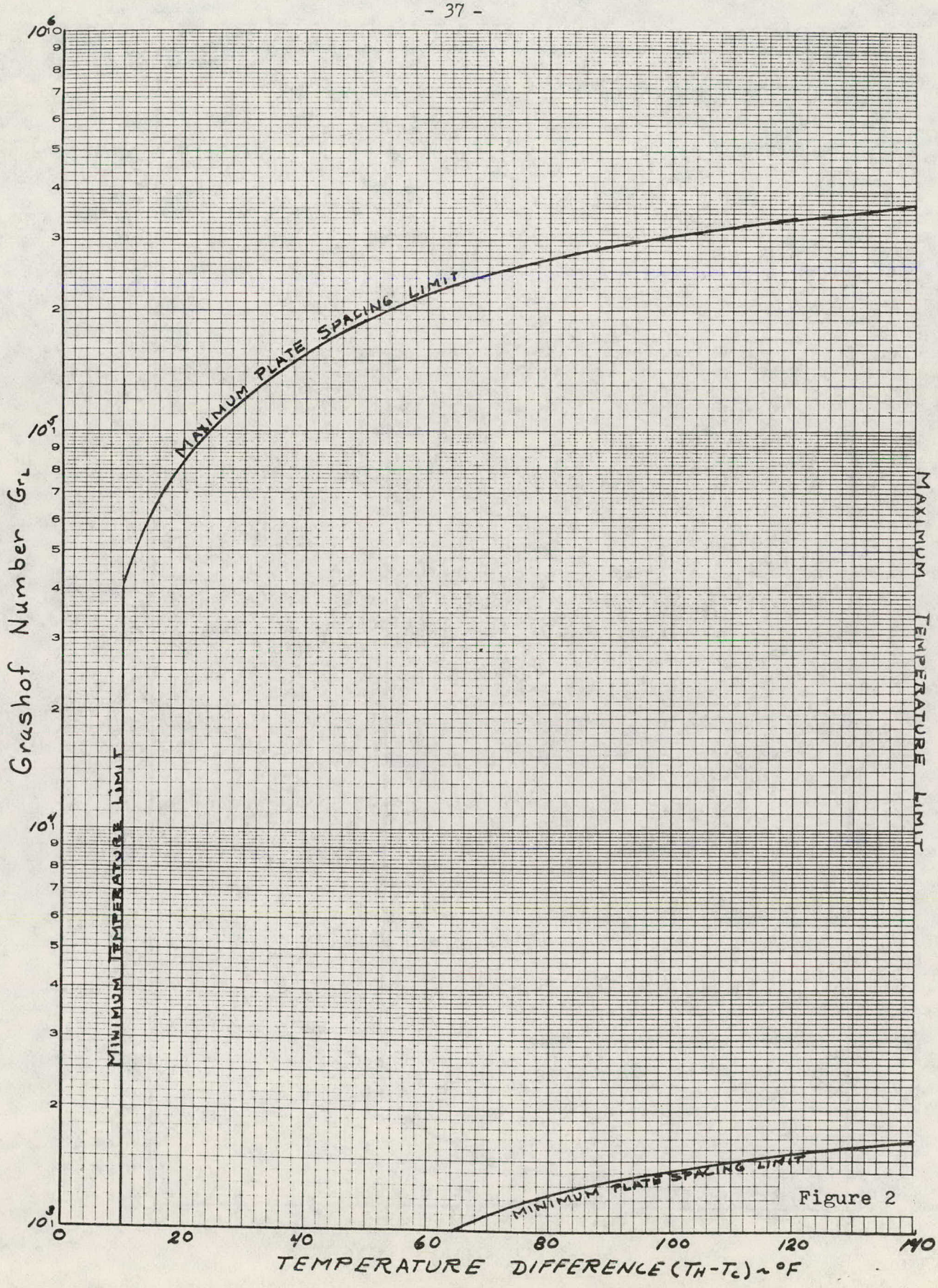
Grashof Number Gr_L
10^6
10^5
10^4
MAXIMUM PLATE SPACING LIMIT
MINIMUM TEMPERATURE LIMIT
MAXIMUM TEMPERATURE LIMIT
MINIMUM PLATE SPACING LIMIT
0
20
40
60
80
100
120
140
TEMPERATURE DIFFERENCE $(T_H - T_C)$ ~ °F

Figure 2

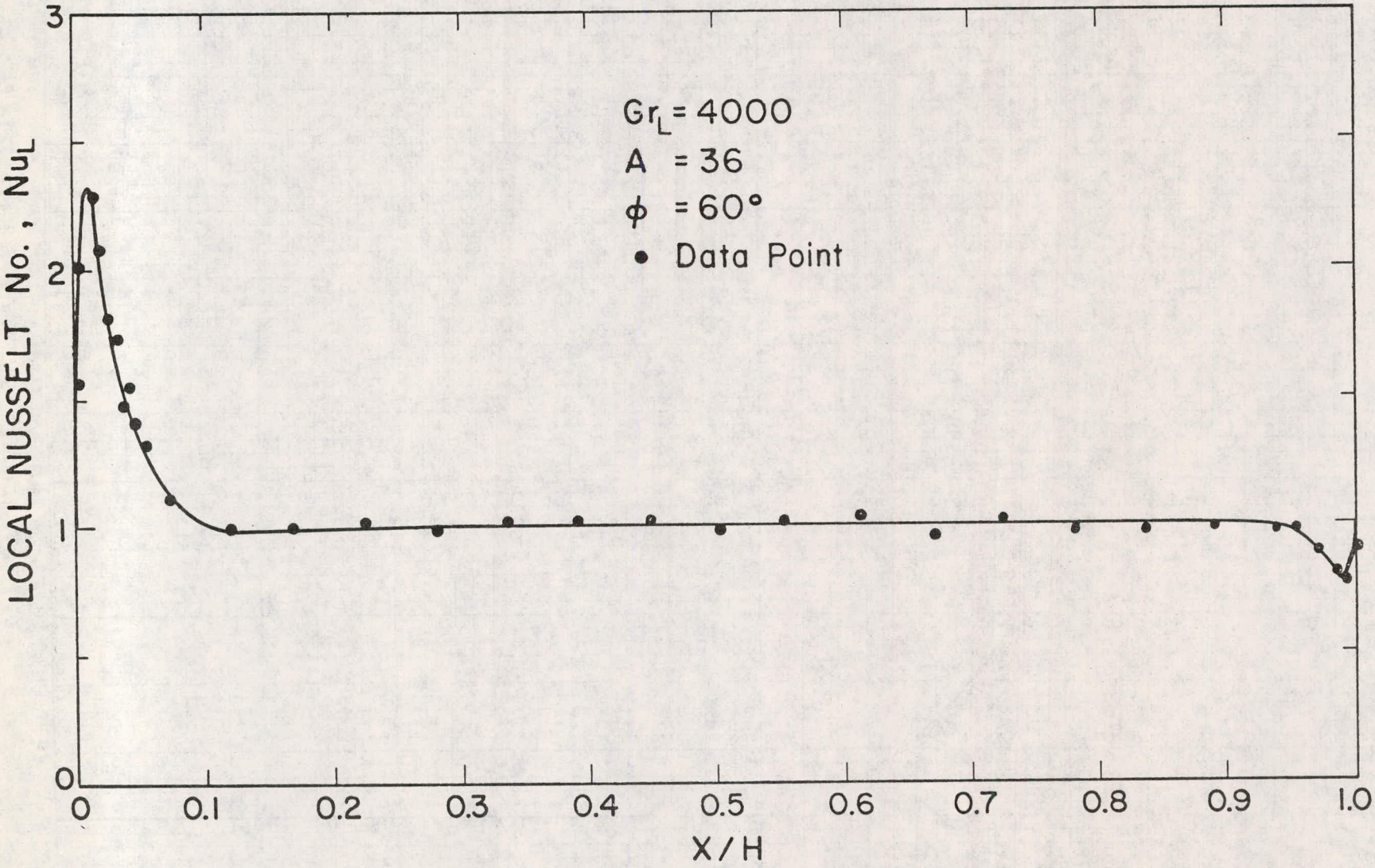
LOCAL NUSSELT No., Nu_L
$Gr_L = 4000$
A = 36
ϕ = 60°
• Data Point
3
2
1
0
0
0.1
0.2
0.3
0.4
0.5
0.6
0.7
0.8
0.9
1.0
X/H

Figure 3

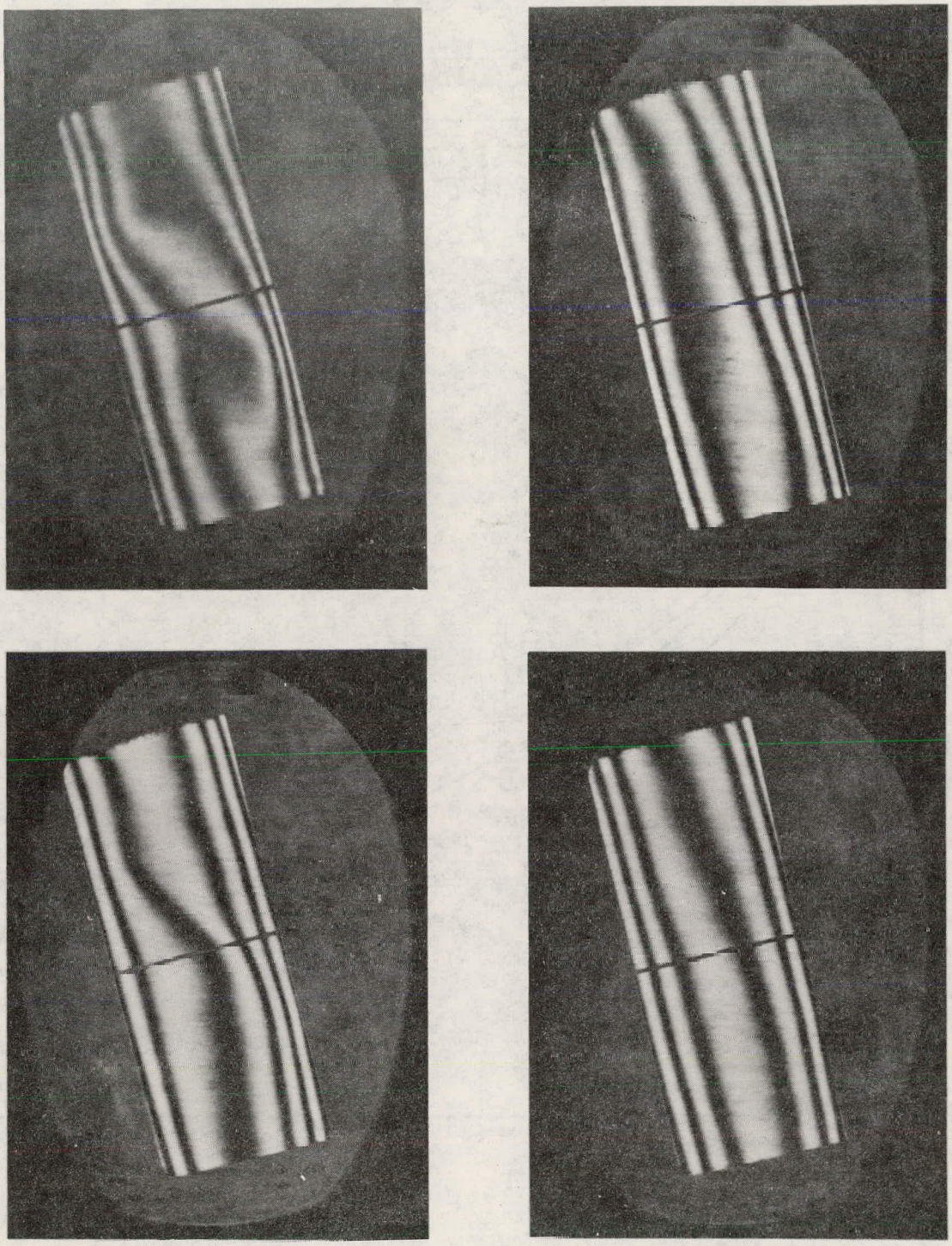

Figure 5: Interferograms taken at random times showing eddy effect at cavity mid-height for Gr_L=26000, A=24. Dark lines are lines of constant temperature.

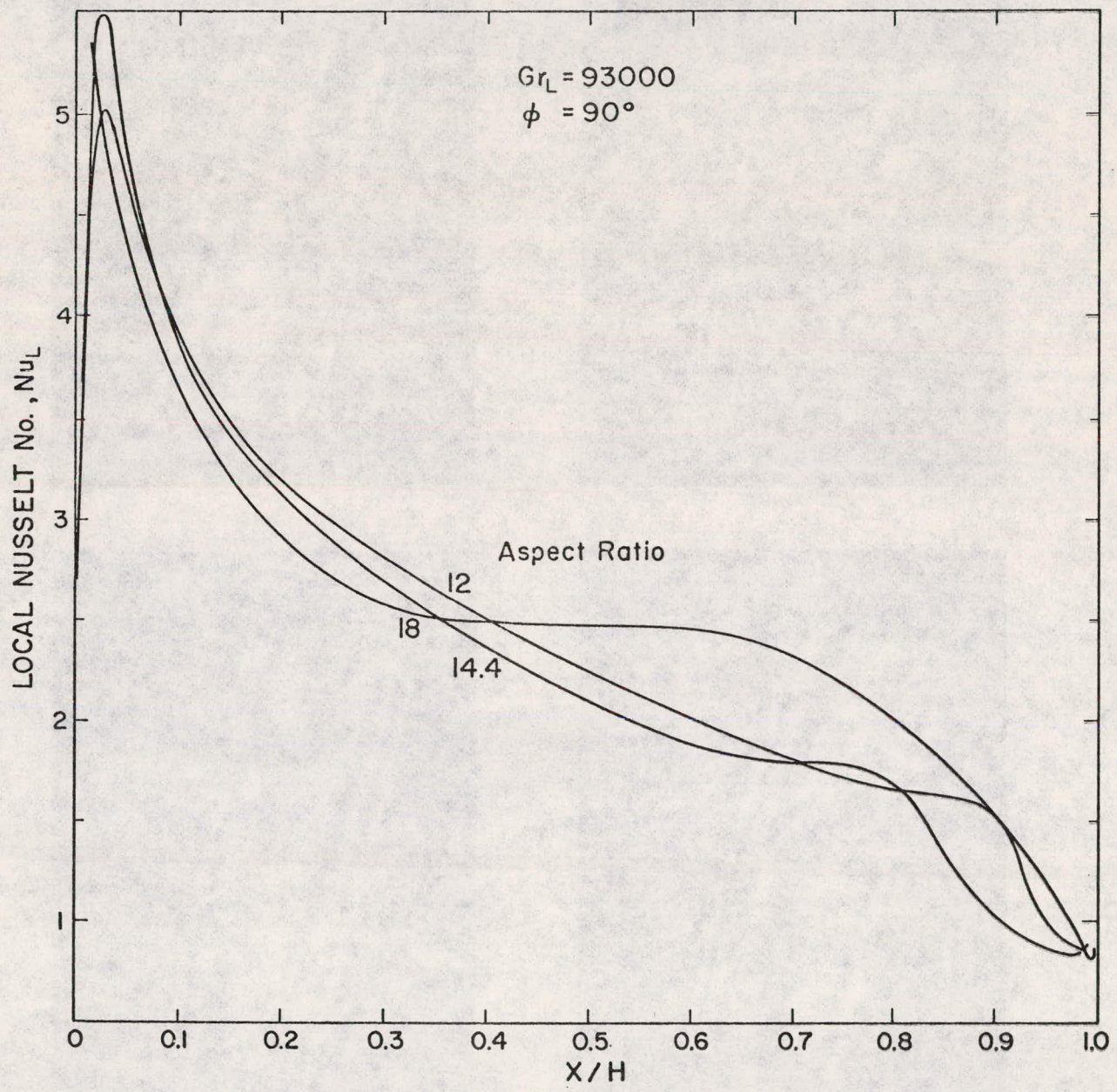
$Gr_L = 93000$
$\phi = 90°$
Aspect Ratio
12
18
14.4
LOCAL NUSSELT No., Nu_L
X/H
0
0.1
0.2
0.3
0.4
0.5
0.6
0.7
0.8
0.9
1.0
1
2
3
4
5

Figure 4

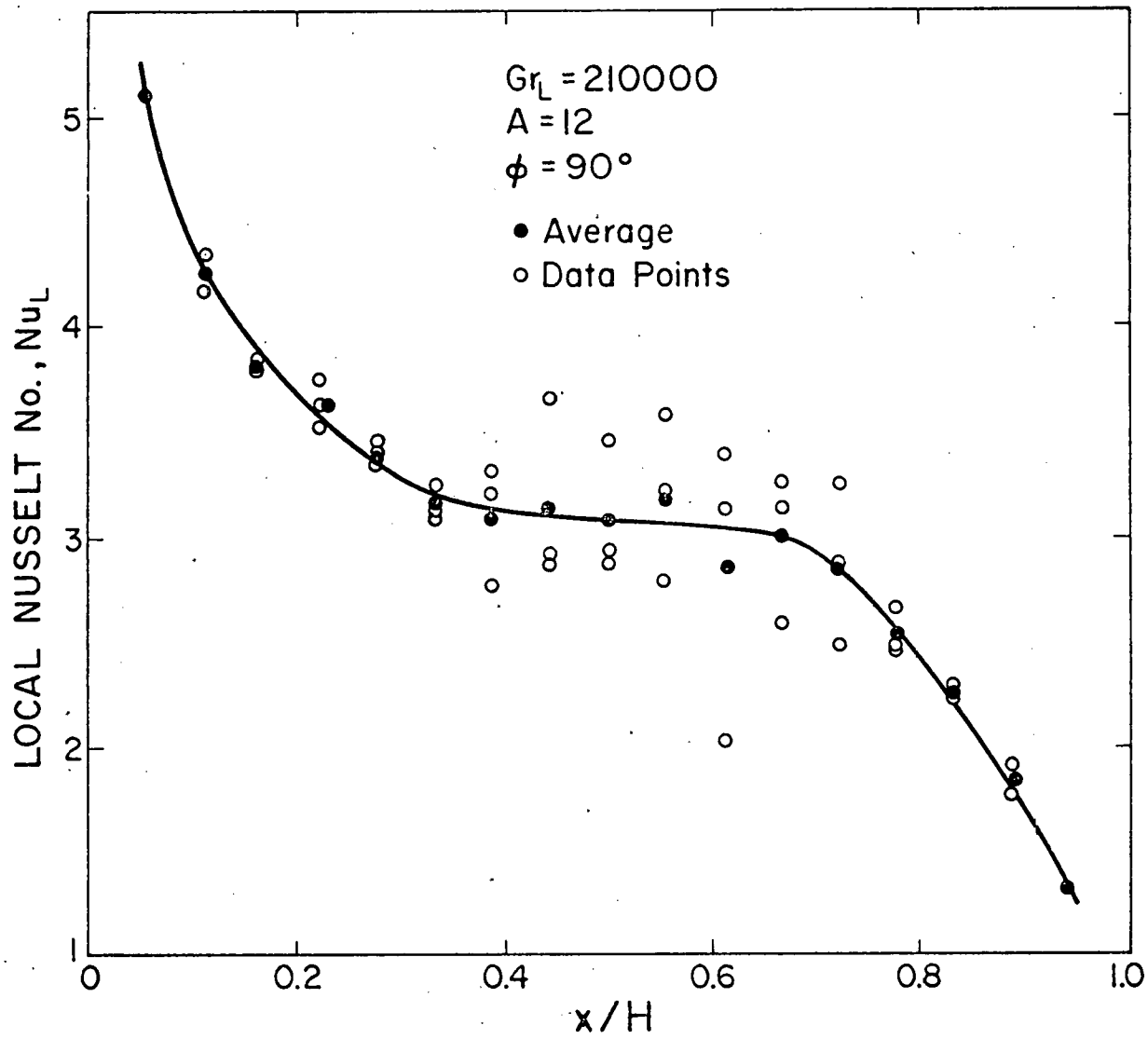
$Gr_L = 210000$
A = 12
$\phi = 90°$
● Average
○ Data Points
LOCAL NUSSELT No., Nu_L
x/H
0
0.2
0.4
0.6
0.8
1.0
1
2
3
4
5

Figure 6

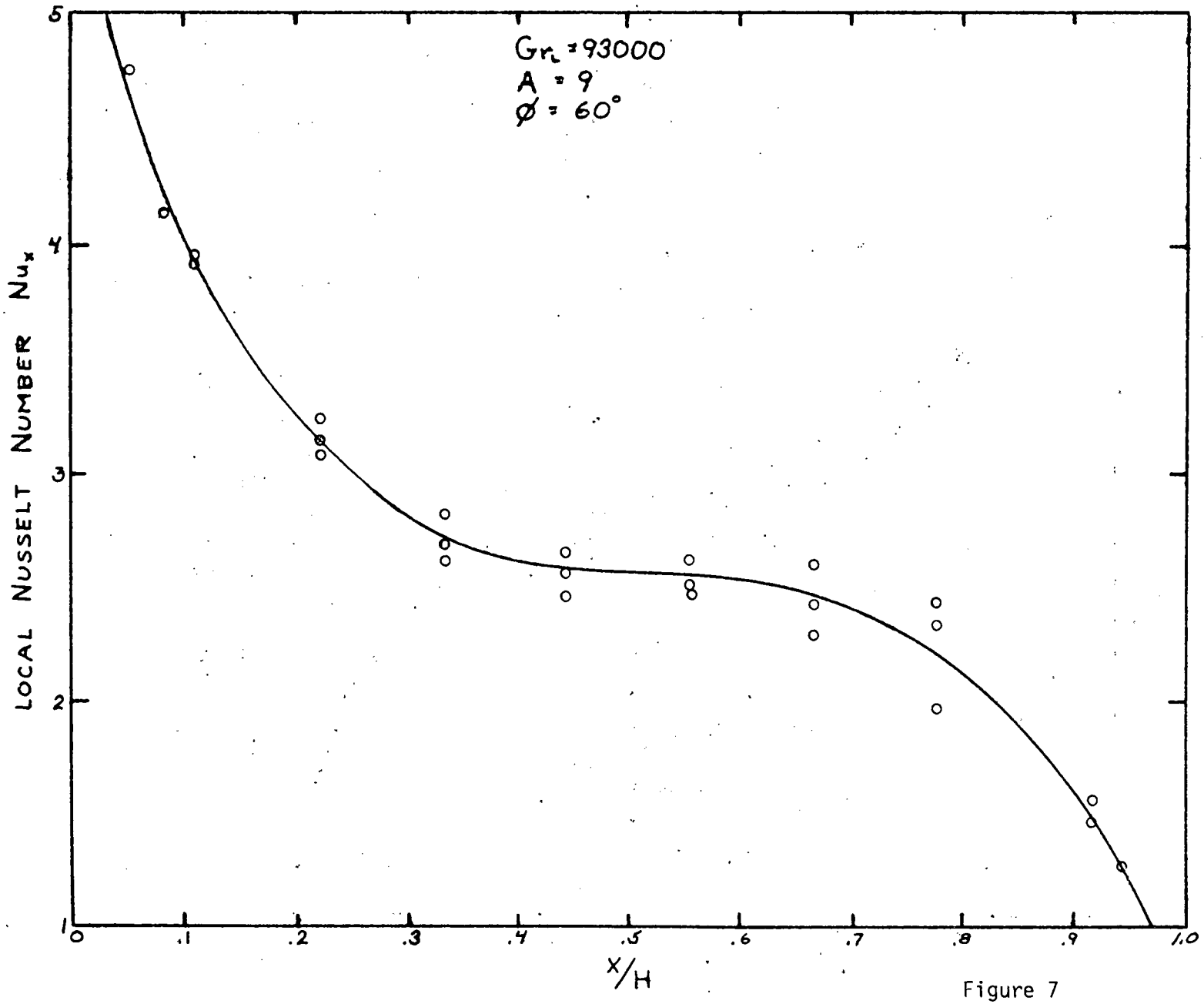
Gr_L = 93000
A = 9
ϕ = 60°
LOCAL NUSSELT NUMBER Nu_x
X/H
5
4
3
2
1
0
.1
.2
.3
.4
.5
.6
.7
.8
.9
1.0

Figure 7

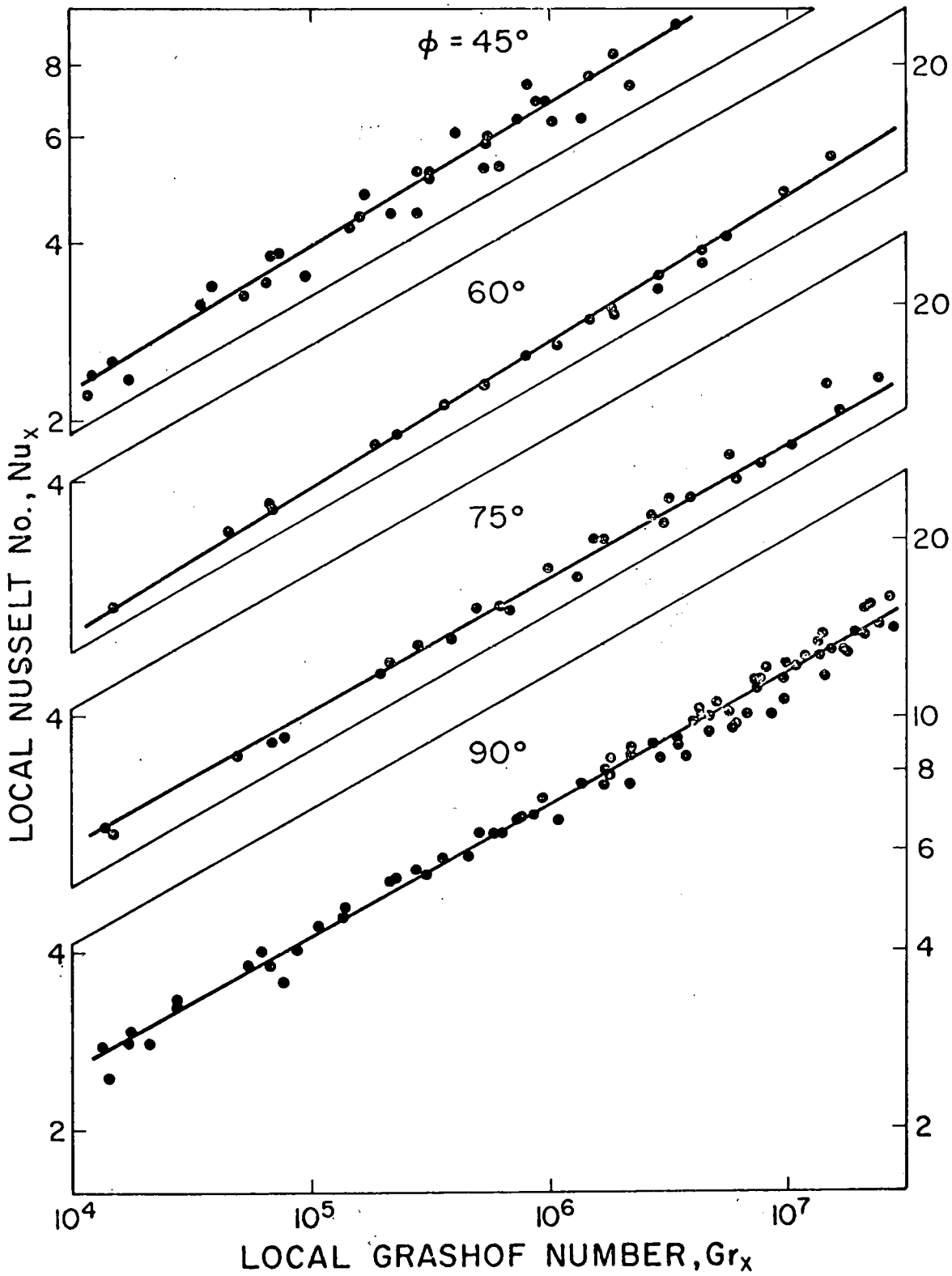
$\phi = 45°$
60°
75°
90°
LOCAL NUSSELT No., Nu_x
LOCAL GRASHOF NUMBER, Gr_x
10^4
10^5
10^6
10^7
2
4
6
8
10
20

Figure 8

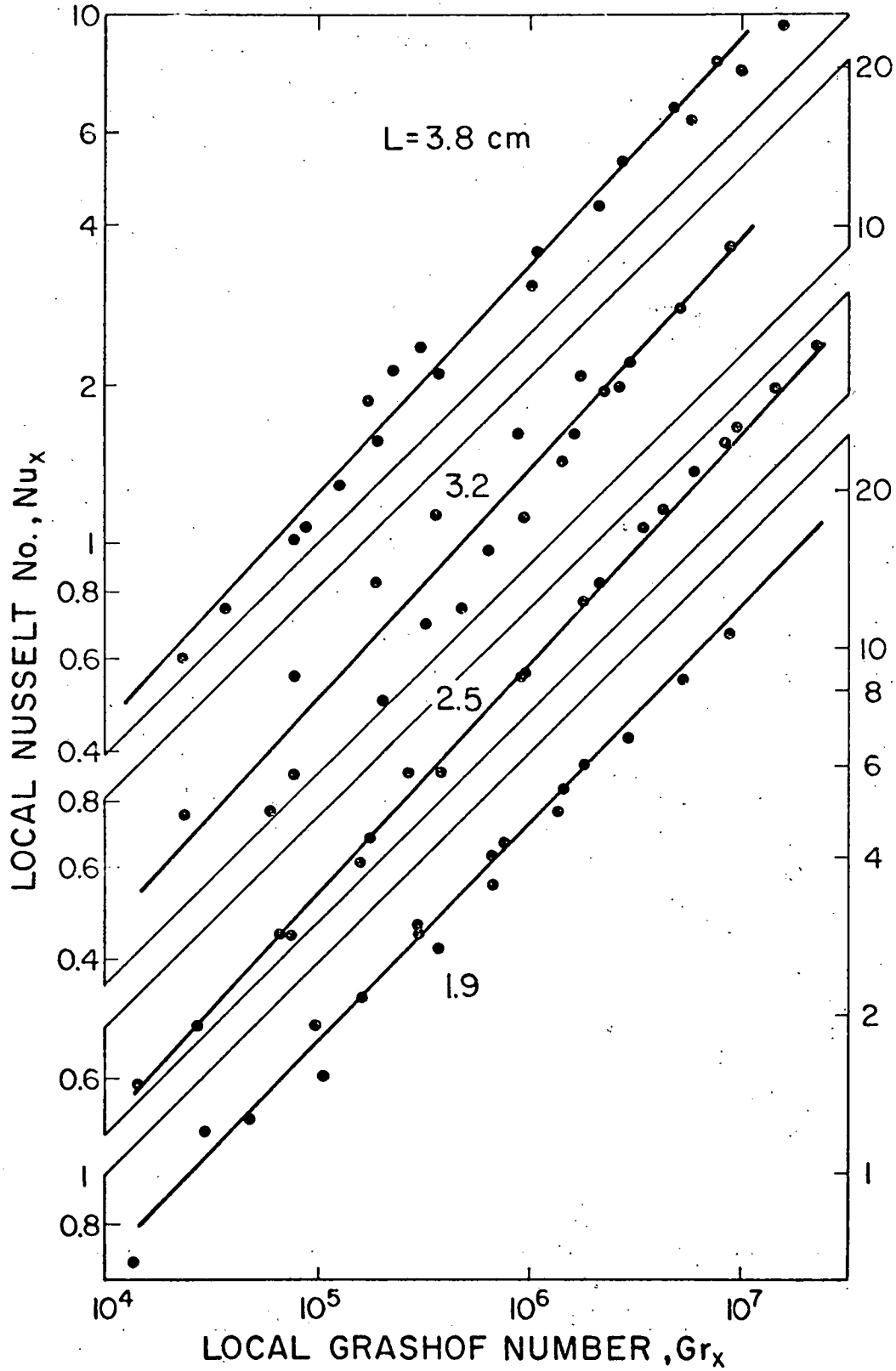
L=3.8 cm
3.2
2.5
1.9
LOCAL NUSSELT No., Nu_x
LOCAL GRASHOF NUMBER, Gr_x
10
6
4
2
1
0.8
0.6
0.4
0.8
0.6
0.4
0.6
1
0.8
20
10
20
10
8
6
4
2
1
10^4
10^5
10^6
10^7

Figure 9

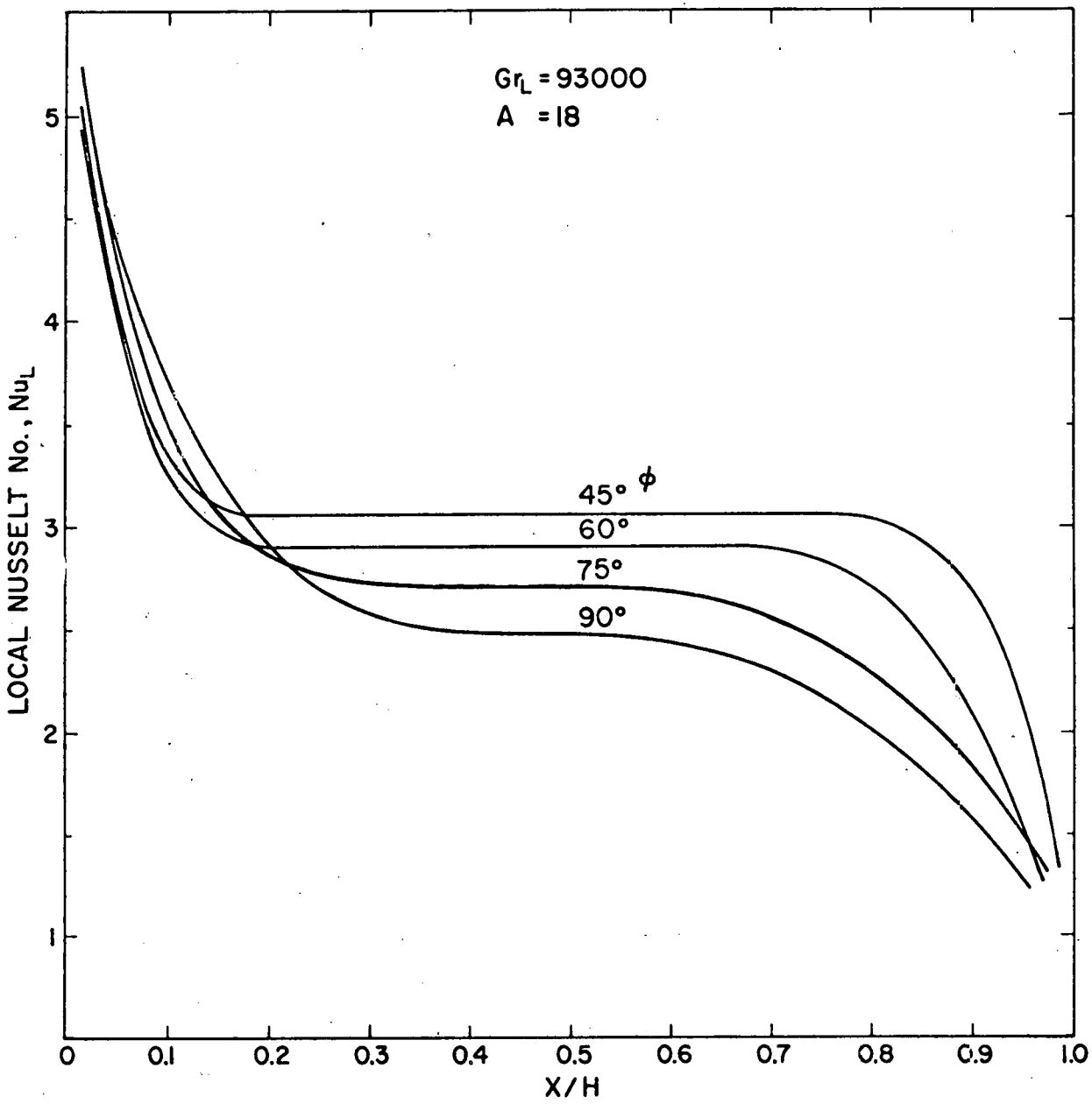
$Gr_L = 93000$
A = 18
45° ϕ
60°
75°
90°
LOCAL NUSSELT No., Nu_L
X/H
0
0.1
0.2
0.3
0.4
0.5
0.6
0.7
0.8
0.9
1.0
1
2
3
4
5

Figure 10

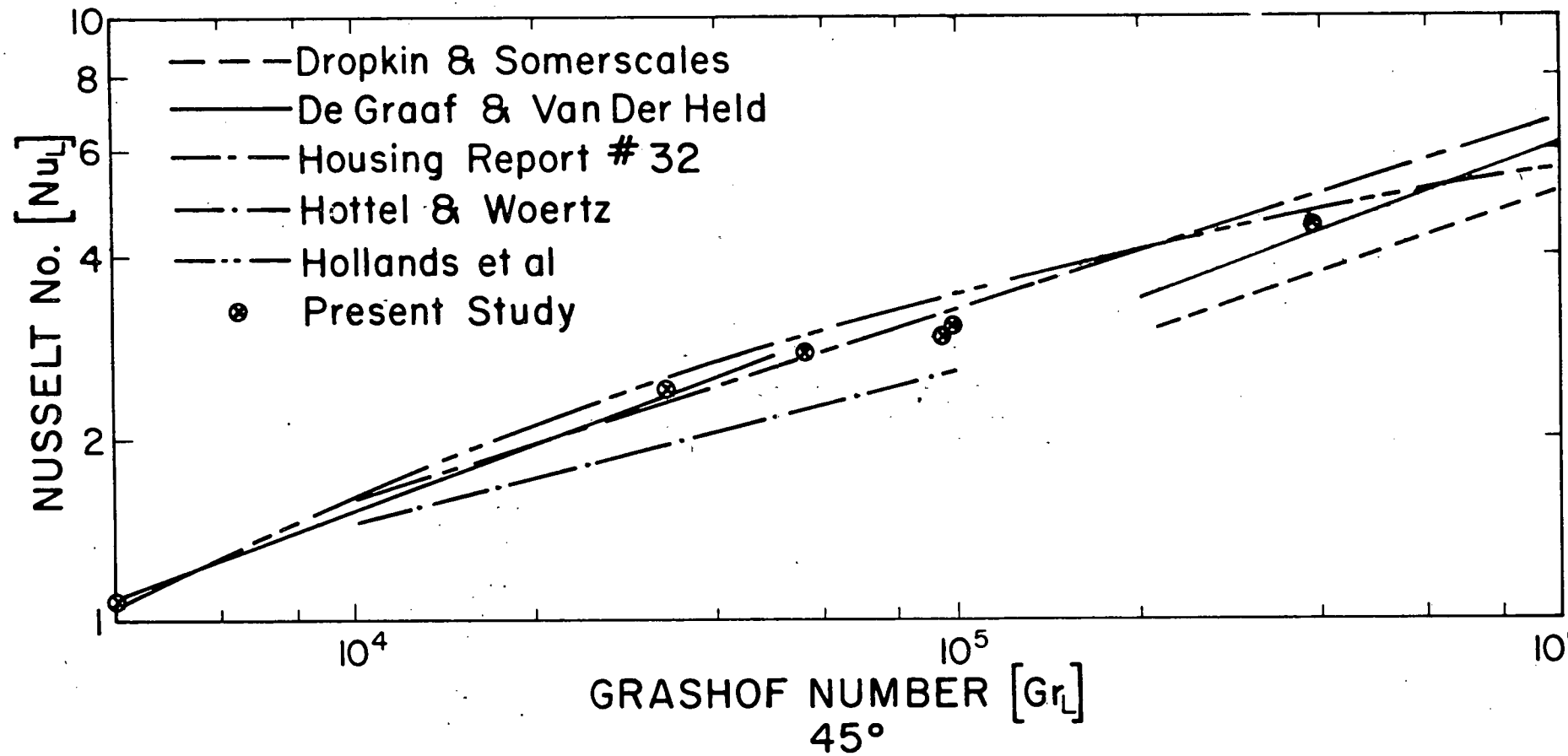
Dropkin & Somerscales
De Graaf & Van Der Held
Housing Report # 32
Hottel & Woertz
Hollands et al
Present Study
NUSSELT No. [Nu_L]
GRASHOF NUMBER [Gr_L]
45°
10
8
6
4
2
1
10^4
10^5
10^6

Figure 11

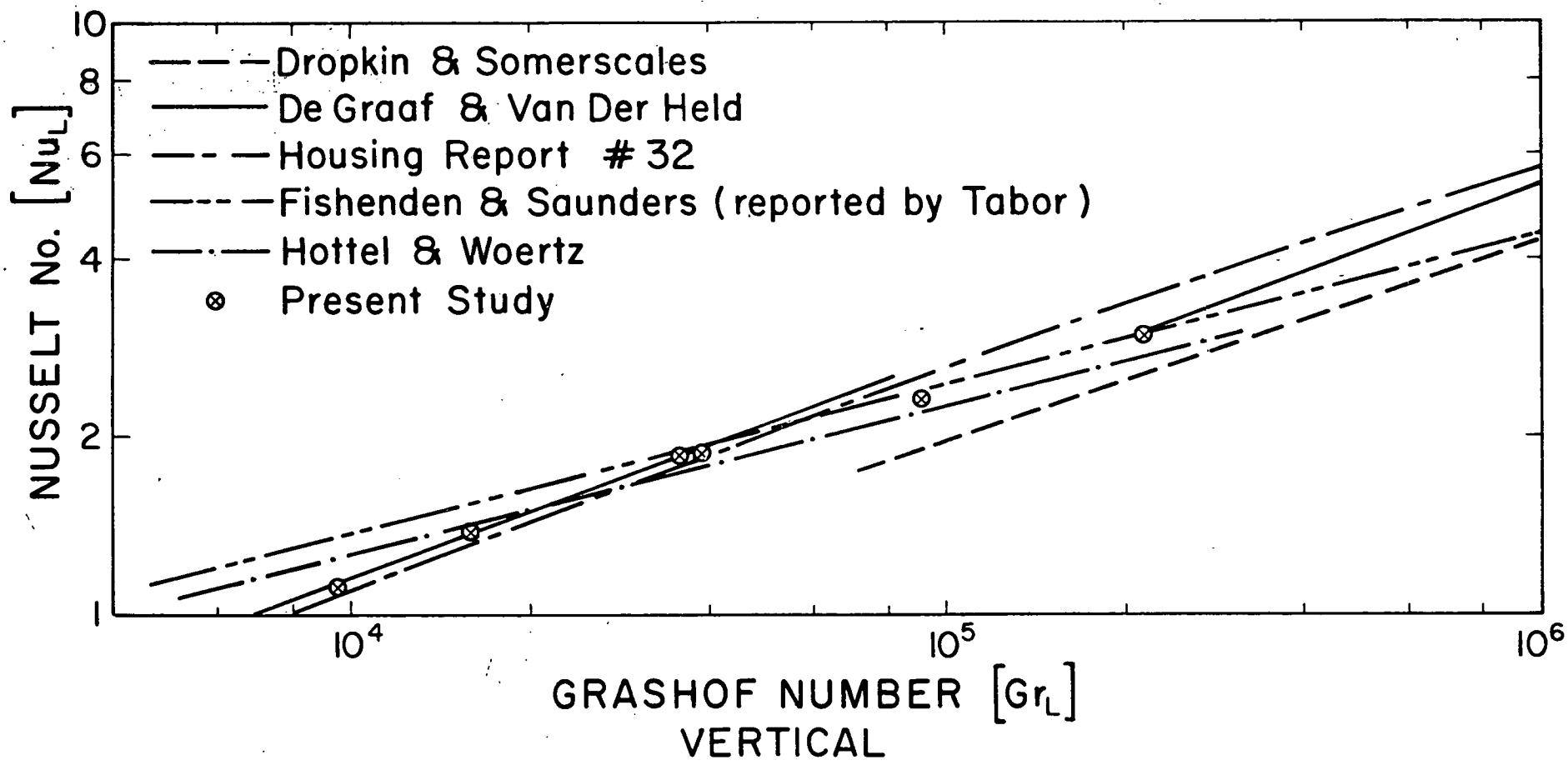
Dropkin & Somerscales
De Graaf & Van Der Held
Housing Report #32
Fishenden & Saunders (reported by Tabor)
Hottel & Woertz
Present Study
NUSSELT No. [Nu_L]
10
8
6
4
2
1
10^4
10^5
10^6
GRASHOF NUMBER [Gr_L]
VERTICAL

Figure 12

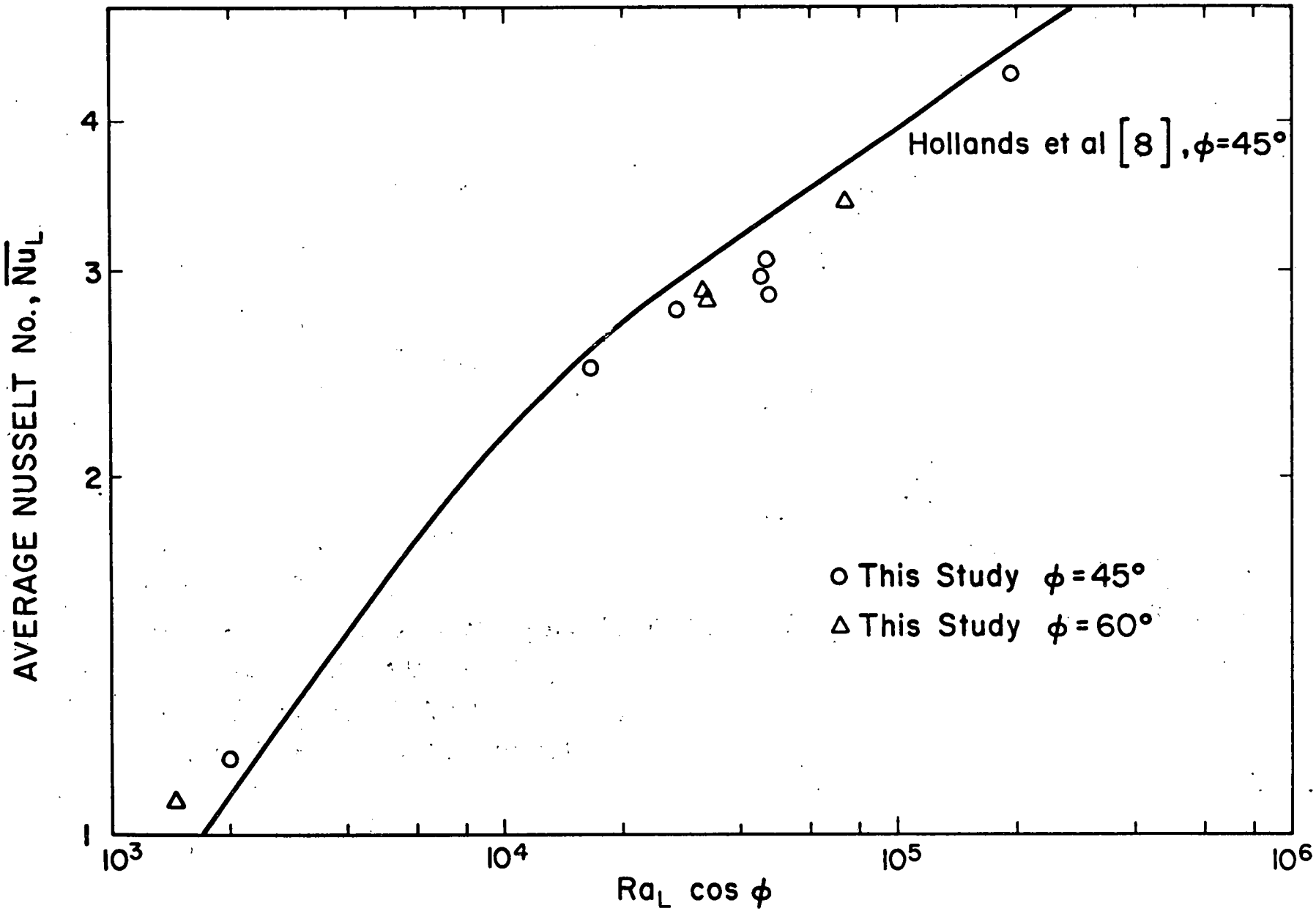
AVERAGE NUSSELT No., $\overline{Nu}_L$
$Ra_L \cos\phi$
Hollands et al [8], ϕ=45°
o This Study ϕ=45°
Δ This Study ϕ=60°
1
2
3
4
10^3
10^4
10^5
10^6

Figure 13

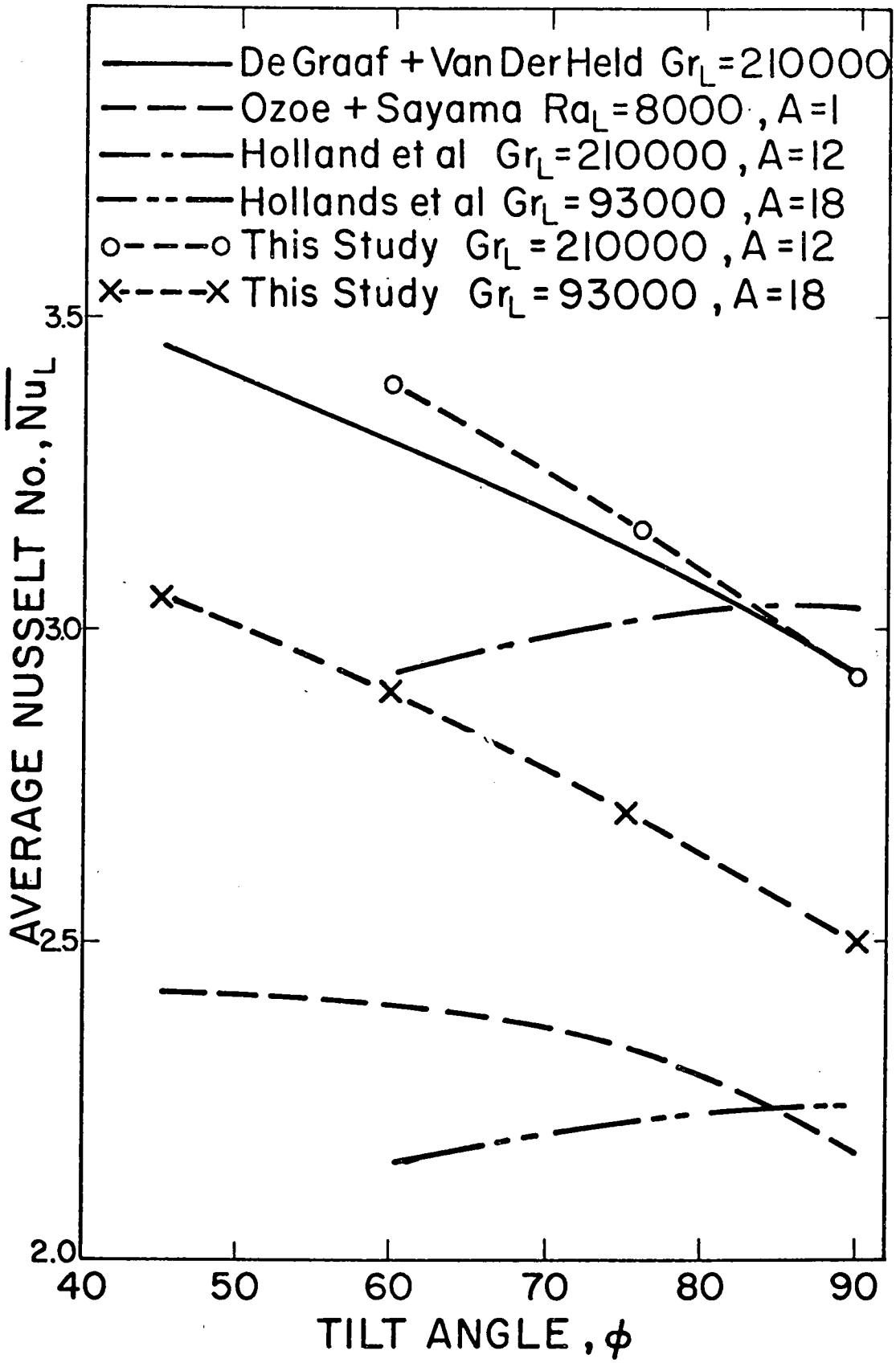
De Graaf + Van Der Held $Gr_L = 210000$
Ozoe + Sayama $Ra_L = 8000$, A = 1
Holland et al $Gr_L = 210000$, A = 12
Hollands et al $Gr_L = 93000$, A = 18
This Study $Gr_L = 210000$, A = 12
This Study $Gr_L = 93000$, A = 18
AVERAGE NUSSELT No., $\overline{Nu}_L$
3.5
3.0
2.5
2.0
40
50
60
70
80
90
TILT ANGLE, ϕ

Figure 14

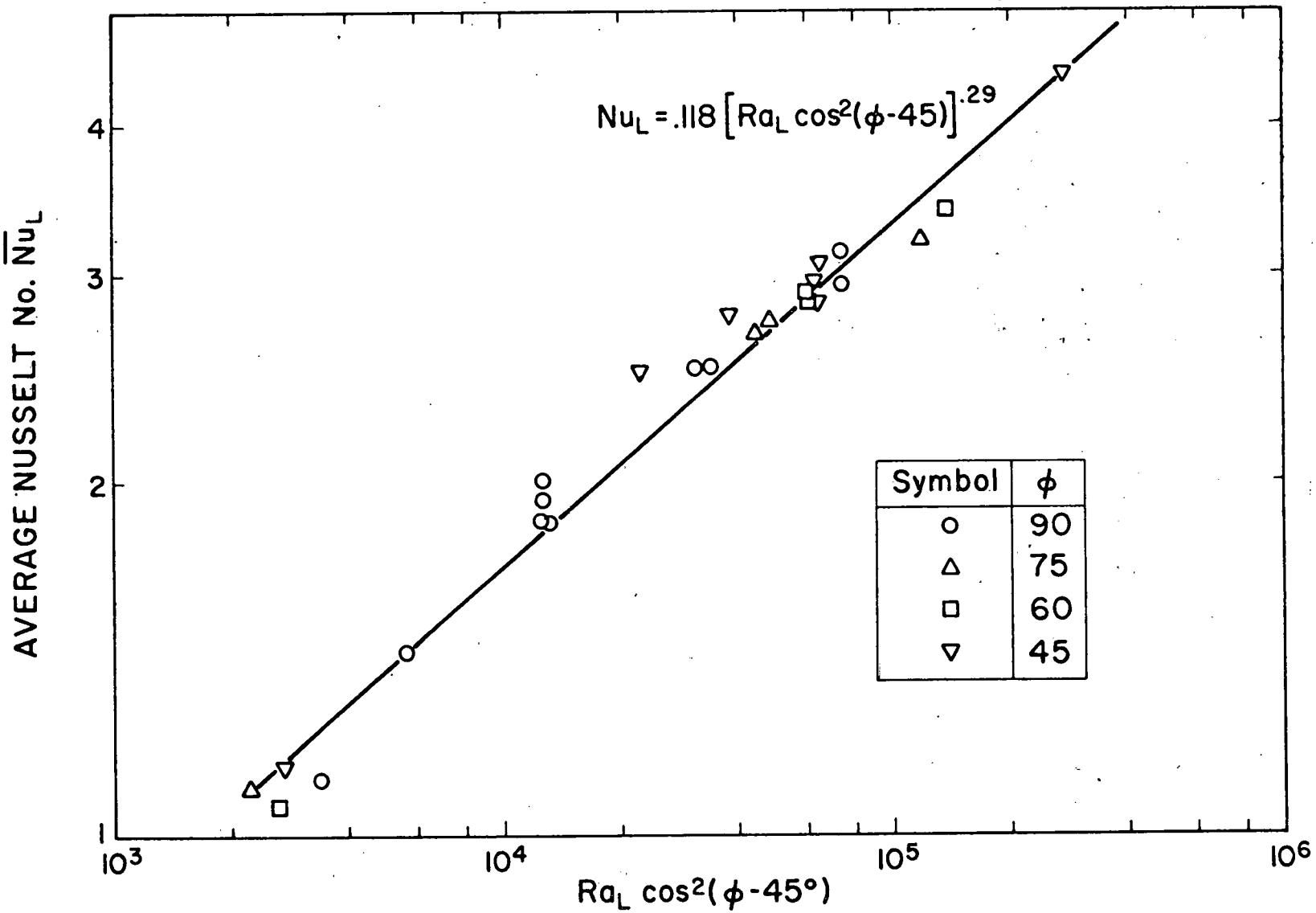

Figure 15

*U.S. GOVERNMENT PRINTING OFFICE: 1977-743-961/4343, Region 4.